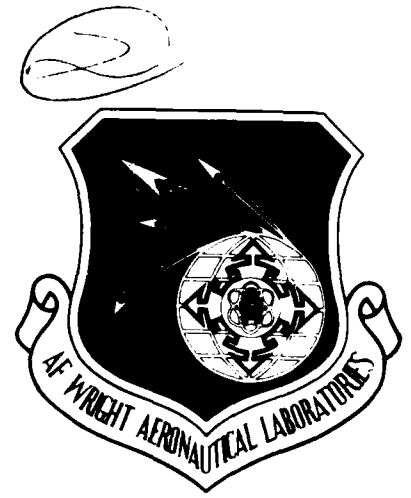


AFWAL-TR-88-3040

AD-A208 277



A VOLTERRA SERIES SUBMODEL APPROACH TO MODELLING
NONLINEAR AERODYNAMICS SYSTEMS

W.T. BAUMANN
T.O. HERDMAN
H.L. STALFORD
F.E. GARRETT

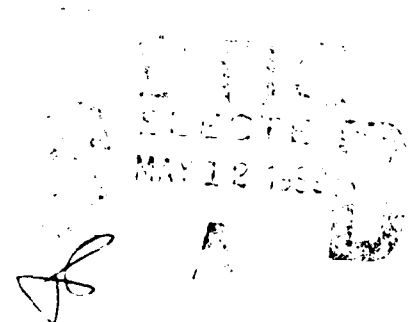
Virginia Polytechnic Institute
and State University
Interdisciplinary Center for Applied
Mathematics
Blacksburg, VA 24061

May 1988

Final Report for Period July 86 to July 87

Approved for public release; distribution unlimited

FLIGHT DYNAMICS LABORATORY
AIR FORCE WRIGHT AERONAUTICAL LABORATORIES
AIR FORCE SYSTEMS COMMAND
WRIGHT-PATTERSON AIR FORCE BASE, OHIO 45433-6553

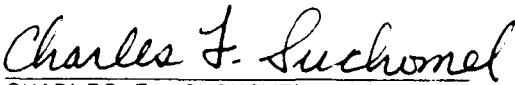



NOTICE

When Government drawings, specifications, or other data are used for any purpose other than in connection with a definitely Government-related procurement, the United States Government incurs no responsibility or any obligation whatsoever. The fact that the government may have formulated or in any way supplied the said drawings, specifications, or other data, is not to be regarded by implication, or otherwise in any manner construed, as licensing the holder, or any other person or corporation; or as conveying any rights or permission to manufacture, use, or sell any patented invention that may in any way be related thereto.

This report is releasable to the National Technical Information Service (NTIS). At NTIS, it will be available to the general public, including foreign nations.

This technical report has been reviewed and is approved for publication.


CHARLES F. SUCHOMEL
Project Engineer
Control Dynamics Branch
Flight Control Division


DAVID K. BOWSER, Chief
Control Dynamics Branch
Flight Control Division

FOR THE COMMANDER


H. MAX DAVIS, Assistant for
Research and Technology
Flight Control Division
Flight Dynamics Laboratory

If your address has changed, if you wish to be removed from our mailing list, or if the addressee is no longer employed by your organization please notify AFWAL/FIGC, Wright-Patterson AFB, OH 45433-6553 to help us maintain a current mailing list.

Copies of this report should not be returned unless return is required by security considerations, contractual obligations, or notice on a specific document.

UNCLASSIFIED

SECURITY CLASSIFICATION OF THIS PAGE

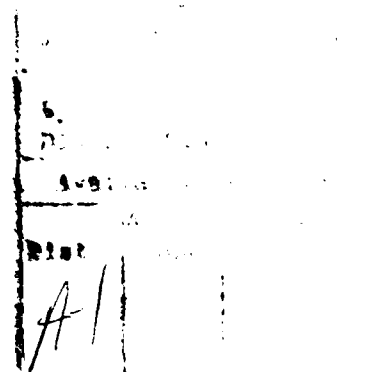
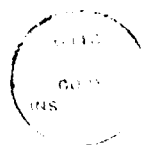
REPORT DOCUMENTATION PAGE

Form Approved
OMB No. 0704-0188

1a. REPORT SECURITY CLASSIFICATION UNCLASSIFIED			1b. RESTRICTIVE MARKINGS N/A	
2a. SECURITY CLASSIFICATION AUTHORITY N/A			3. DISTRIBUTION / AVAILABILITY OF REPORT Approved for public release; distribution is unlimited.	
2b. DECLASSIFICATION / DOWNGRADING SCHEDULE N/A				
4. PERFORMING ORGANIZATION REPORT NUMBER(S) NONE			5. MONITORING ORGANIZATION REPORT NUMBER(S) AFWAL-TR-88-3040	
6a. NAME OF PERFORMING ORGANIZATION Virginia Polytechnic Institute and State University		6b. OFFICE SYMBOL (If applicable)	7a. NAME OF MONITORING ORGANIZATION Flight Dynamics Laboratory (AFWAL/FIGG AF Wright Aeronautical Laboratories	
6c. ADDRESS (City, State, and ZIP Code) Blacksburg, Virginia 24061			7b. ADDRESS (City, State, and ZIP Code) Wright-Patterson AFB, Ohio 45433-6553	
8a. NAME OF FUNDING / SPONSORING ORGANIZATION Air Force Wright Aeronautical Laboratories		8b. OFFICE SYMBOL (If applicable) FIGCB	9. PROCUREMENT INSTRUMENT IDENTIFICATION NUMBER F33615-86-K-3617	
6c. ADDRESS (City, State, and ZIP Code) Wright Patterson AFB, Ohio 45433-6553			10. SOURCE OF FUNDING NUMBERS	
			PROGRAM ELEMENT NO 01102F	PROJECT NO 2307
			TASK NO NS	WORK UNIT ACCESSION NO 26
11. TITLE (Include Security Classification) A Volterra Series Submodel Approach to Modelling Nonlinear Aerodynamics Systems				
12. PERSONAL AUTHOR(S) W.T. Baumann, T. L. Herdman, H. L. Stalford, F.E. Garrett				
13a. TYPE OF REPORT Final		13b. TIME COVERED FROM July 86 TO July 87		14. DATE OF REPORT (Year, Month, Day) 1988, May
15. PAGE COUNT 70				
16. SUPPLEMENTARY NOTATION				
17. COSATI CODES			18. SUBJECT TERMS (Continue on reverse if necessary and identify by block number)	
FIELD	GROUP	SUB-GROUP		
	03		Nonlinear Flying Qualities Nonlinear Dynamics	
	01		Nonlinear Systems Theory High Angle-of-Attack	
			Volterra Series	
19. ABSTRACT (Continue on reverse if necessary and identify by block number) High performance aircraft have mission requirements for operating in high angle-of-attack and sideslip conditions and in various maneuvers of unsteady, large amplitudes governed by multiple-input, multiple-output nonlinear dynamics. The large amplitudes coupled with high degree nonlinear dynamics lead to requirements for nonlinear flying qualities. These qualities require analyses of nonlinear dynamic stability, nonlinear control, and nonlinear response behavior of such aircraft. Techniques are needed that (1) are computationally feasible, (2) retain the nonlinearities of the aircraft and (3) provide physical and mathematical understanding of the important nonlinear flying qualities. This report documents the results of efforts to develop such techniques using the Volterra Series representation for nonlinear aircraft models of high α flight.				
20. DISTRIBUTION / AVAILABILITY OF ABSTRACT <input checked="" type="checkbox"/> UNCLASSIFIED/UNLIMITED <input type="checkbox"/> SAME AS RPT <input type="checkbox"/> DTIC USERS			21. ABSTRACT SECURITY CLASSIFICATION UNCLASSIFIED	
22a. NAME OF RESPONSIBLE INDIVIDUAL Charles F. Suchomel			22b. TELEPHONE (Include Area Code) (513) 255-8496	22c. OFFICE SYMBOL AFWAL/FIGCB

TABLE OF CONTENTS

1. Introduction	1
2. Volterra Series Representation For Nonlinear Systems	3
3. Simulation Results	6
3.1 Longitudinal Limit Cycle	6
3.2 Wing Rock Limit Cycle	18
4. Analysis	27
4.1 Volterra Series Analysis	27
4.2 Classical Analysis	30
5. Conclusion	40
References	42
List of Symbols	45
Appendix A. Volterra Series Representation	47
Appendix B. Longitudinal Equations of Motion	50
Appendix C. Volterra Expansion for Longitudinal Example	54
Appendix D. Wing Rock Model	56
Appendix E. Expansion of Volterra Series for Wing Rock Example	62
Appendix F. Two-Term Volterra Series Approximation	64
Appendix G. SMP Function for Volterra Equation Calculations	71



FOREWARD

This technical report was prepared by Drs. William Baumann, Terry Herdman, Harold Stalford, and Mr. Frederick Garrett, Jr. This work was performed under the sponsorship of the United States Air Force (USAF), and was administered under the direction of the Air Force Flight Dynamics Laboratory, Air Force Systems Command, Wright-Patterson Air Force Base, Ohio. Mr. Charles F. Suchomel (AFVVAL/FIGC) was the Project Engineer for the Air Force. This report represents a part of the task to identify a technique that describes nonlinear aircraft dynamic properties potentially useful as flying quality indicators in large-amplitude and/or high-acceleration motions. This work was accomplished over the period 16 July 1986 through 15 July 1987.

1. Introduction

High performance aircraft have mission requirements for operating in high angle-of-attack and sideslip conditions and in various maneuvers of unsteady, large amplitudes governed by multiple-input, multiple-output nonlinear dynamics. The large amplitudes coupled with high degree nonlinear dynamics lead to requirements for nonlinear flying qualities. These qualities require analyses of nonlinear dynamic stability, nonlinear control, and nonlinear response behavior of such aircraft. Techniques are needed that (1) are computationally feasible, (2) retain the nonlinearities of the aircraft and (3) provide physical and mathematical understanding of the important nonlinear flying qualities.

One methodology which has recently exhibited promising evidence of accomplishing the above is the Volterra Series. The purpose of this project is to obtain Volterra series representations of nonlinear systems typical of high performance aircraft in large amplitude maneuvers.

The development of the Volterra representation for the six DOF (degree of freedom) rigid body-equations of motion is given in [1]. Therein, the nonlinear equations of motion are formulated using the four-parameter (quaternions) method (see [2,3,4]). The first three terms of the Volterra Series representation are constructed in [5] for the longitudinal motion of the F-8 crusader aircraft using the nonlinear model developed by Garrard and Jordan [6]. Suchomel [5] has numerically evaluated the three-term Volterra Series representation of an extended version of Garrard and Jordan's model which incorporated some additional aerodynamic drag and thrust terms. Suchomel's work compares the predictive performance of the three-term Volterra Series representation against the Runge-Kutta integration of the full nonlinear model. His results demonstrate that the approximating three-term Volterra Series gives an accurate prediction of the output response of the given nonlinear system.

The present work continues the application of the Volterra Series representation [1] to nonlinear aircraft models of high α flight. The nonlinear models of such flight have natural low-order submodels which hold over separate flight regimes (e.g., pre-stall, stall and post-

stall). For example, in the pre-stall regime we observe an almost linear relationship between the state variables and the aerodynamic force and moment coefficients. In the stall and post-stall regimes the relationship becomes a combination of linear, bilinear, quadratic, cubic, etc. It is not only necessary but unnatural to search for a single high-order, nonlinear relationship that governs flight behavior in the total envelope spanning pre-stall, stall and post-stall flight. It is, however, feasible to provide simple low-order dynamics that govern each separate flight regime and then combine them to form the total nonlinear model. The total then consists of a set of simple low-order equations that govern flight in each regime (or subspace) and that agree with the equations of the adjoining regime at their common boundaries. In this work we consider such subspace models. They come about naturally as described above.

In Section 3.1 we consider a nonlinear wind tunnel model for high alpha (α) longitudinal flight involving the limit cycle. We show how the complex nonlinear aerodynamic model has a natural representation in terms of linear and quadratic subspace models which have fairly simple Volterra Series representations. Simulation analysis is conducted on both the original nonlinear windtunnel model and the Volterra subspace approximation. The accuracy of the approximation is investigated.

Next, in Section 3.2, we consider a nonlinear windtunnel model of wing rock which is generated by unsteady aerodynamics effects [23-33]. The complex model is a simple composition of two bilinear subspace models. Again, simulation analysis is conducted and the accuracy of the approximation is investigated.

Section 4 considers methods for analyzing the nonlinear responses discussed in Section 3. In 4.1 an approach based on Volterra models is discussed. The application of classic analysis techniques to the same models of Section 3 is explored in Section 4.2.

Our conclusions and suggestions for future research are contained in Section 5.

2. Volterra Series Representation For Nonlinear Systems

The first approach usually taken when confronted with the task of analyzing a nonlinear system of ordinary differential equations is to linearize. However, some current flight dynamics problems of interest to the Air Force possess significant nonlinearities in the complete mathematical model that cannot be ignored. To predict the behavioral characteristics of the system, the complete nonlinear model, or at least an approximation that contains the significant nonlinearities, must be analyzed.

The well-developed theory of differential equations has provided general existence and uniqueness results for nonlinear systems. However, these results, unlike the corresponding results for linear systems, do not provide a closed form representation for the solution. The mathematical tools for the analysis of nonlinear systems are limited, and the known techniques are not well developed when compared to the results for linear systems.

One technique for the study of nonlinear systems that has shown promise is the Volterra series approach [1,5,7-19]. This approach provides a series representation for the input-output behavior of the nonlinear system. In particular, the Volterra series gives a mathematical representation of the solution in the form of an expanding infinite series of integrals which encompasses the nonlinearities of the system. This representation can be viewed as a series in which each term is the solution of a linear equation where the nonlinearities of the system appear as forcing functions. For a nonlinear differential equation of the form

$$\dot{x} = f(x, u)$$

the Volterra series representation of the solution is an infinite series of integrals

$$\begin{aligned} x(t) = & h_0(t) + \int_0^t h_1(t - \sigma_1)u(\sigma_1)d\sigma_1 \\ & + \int_0^t \int_0^t h_2(t - \sigma_1, t - \sigma_2)u(\sigma_1)u(\sigma_2)d\sigma_1d\sigma_2 \\ & + \int_0^t \int_0^t \int_0^t h_3(t - \sigma_1, t - \sigma_2, t - \sigma_3)u(\sigma_1)u(\sigma_2)u(\sigma_3)d\sigma_1d\sigma_2d\sigma_3 \\ & + \cdots \end{aligned} \tag{2.1}$$

where $h_0(t)$ is the zero-input solution and the $h_i, i = 1, 2, \dots$, are called the i th order Volterra kernels. For a complete discussion of the Volterra series representation for ordinary differential equations see [20,21]. Also, see Appendix A for additional comments on the Volterra series.

The Volterra series approach provides an approximation for the solution by truncating the series. Such a finite representation gives the response of the system in terms of the input signals, initial conditions, and the stability derivatives of the system. This approximation provides not only a methodology for predicting the behavioral responses of the nonlinear system but also a methodology for the study of how various parameters affect the controllability and stability of the system.

The mathematical theory for the Volterra representation is by no means complete. Although some convergence results for the series representation exist, they are extremely conservative and have not proven useful in engineering applications. In most applications the significant characteristics of the system are contained in the second or third terms; therefore convergence is not a major issue.

Our technique for approximating the solution of nonlinear models of high α flight is based on a subspace concept. The subspaces arise naturally in the aerodynamic forces and moments in high performance flight. Our approach is outlined as follows:

1. partition the total envelope into natural subspaces in which the nonlinearities can be accurately described by low-order multivariable polynomials (preferably third order or less),
2. pick an equilibrium point for each subspace, (we have no definite procedure for selecting the equilibrium point - at present these points are selected in an ad hoc manner),
3. approximate the solution of the differential equation for each subspace by a truncated Volterra series (three terms or less).

For this approach the differential equation form is employed for the terms of the Volterra

series instead of the integral from (see Appendix A). Consider inputs of the form

$$u = u_0 + ku_1$$

where u_0, u_1 denote an equilibrium and a perturbation input. The solution to the nonlinear differential equation has the form, see [20, Chapter three],

$$x = x_0 + kx_1 + k^2x_2 + k^3x_3 + \dots$$

where x is the state, k is a constant, x_0 is the initial equilibrium state and x_i is the contribution to the state from the i th term in the Volterra series. Substituting this representation for the solution x into the governing equation, expanding the right hand side in a Taylor series with respect to k , and equating coefficients of equal powers of k gives rise to the following equations for the first three terms of the Volterra series representation

$$\dot{x}_1 = Ax_1 + bu_1$$

$$\dot{x}_2 = Ax_2 + g_1(x_1), \quad x_2(0) = 0$$

$$\dot{x}_3 = Ax_3 + g_2(x_1, x_2), \quad x_3(0) = 0$$

where A is a $n \times n$ matrix (the state is $n \times 1$), b is a $n \times 1$ vector, and the $g_i, i = 1, 2$ are in general $n \times 1$ nonlinear functions of their variables. All of these quantities depend on the equilibrium point about which the Volterra series is expanded. Upon entering a subspace the state equations are reinitialized by incorporating the current state into the initial condition of the linear part x_1 . In the event that the polynomial of step 1 above is first order, the corresponding, $g_i, i = 1, 2$ are zero and the Volterra series is simply a linear system.

In Appendix G we describe a program that computes the differential equations for each Volterra term. This program was used for all the Volterra equation calculations discussed in this report.

3. Simulation Results

The following examples will serve to illustrate the application of the Volterra series representation to subspace models of nonlinear systems.

3.1 Longitudinal Limit Cycle: Example 1

For the purpose of illustrating our approach, we consider a simplified nonlinear model of the longitudinal limit cycle at high angle of attack, α . Simplified high α flight is governed roughly by the following two differential equations developed in Appendix B

$$\dot{\alpha} = q + 9.168C_z(\alpha) - 1.8336(\delta_e + 7^\circ) + 7.361904 \quad (3.1)$$

$$\dot{q} = 5.73(C_{m_\alpha}\alpha + C_{m_{\delta_e}}\delta_e) + 2.865 \quad (3.2)$$

where α is the angle-of-attack in degrees, q is the pitch rate in degrees per second and δ_e is the elevator control in degrees. To keep the presentation simple, we prescribe $C_{m_\alpha} = -1$ and $C_{m_{\delta_e}} = -1.5$. The nonlinear plunging force coefficient $C_z(\alpha)$ is represented by the following equations (3.3) through (3.6). It has the appearance of an inverted high α lift curve, Figure 3-1. This model in discrete data points was taken from measured wind-tunnel values of the T-2C airplane, Stalford [22]. The coefficients in equations (3.3) through (3.6) were numerically calculated to provide a fit for the discrete data points for the corresponding α intervals.

The slope of the C_z curve is approximately linear up to stall which occurs around $\alpha = 14.5^\circ$. This portion of the C_z curve is represented accurately by the linear function

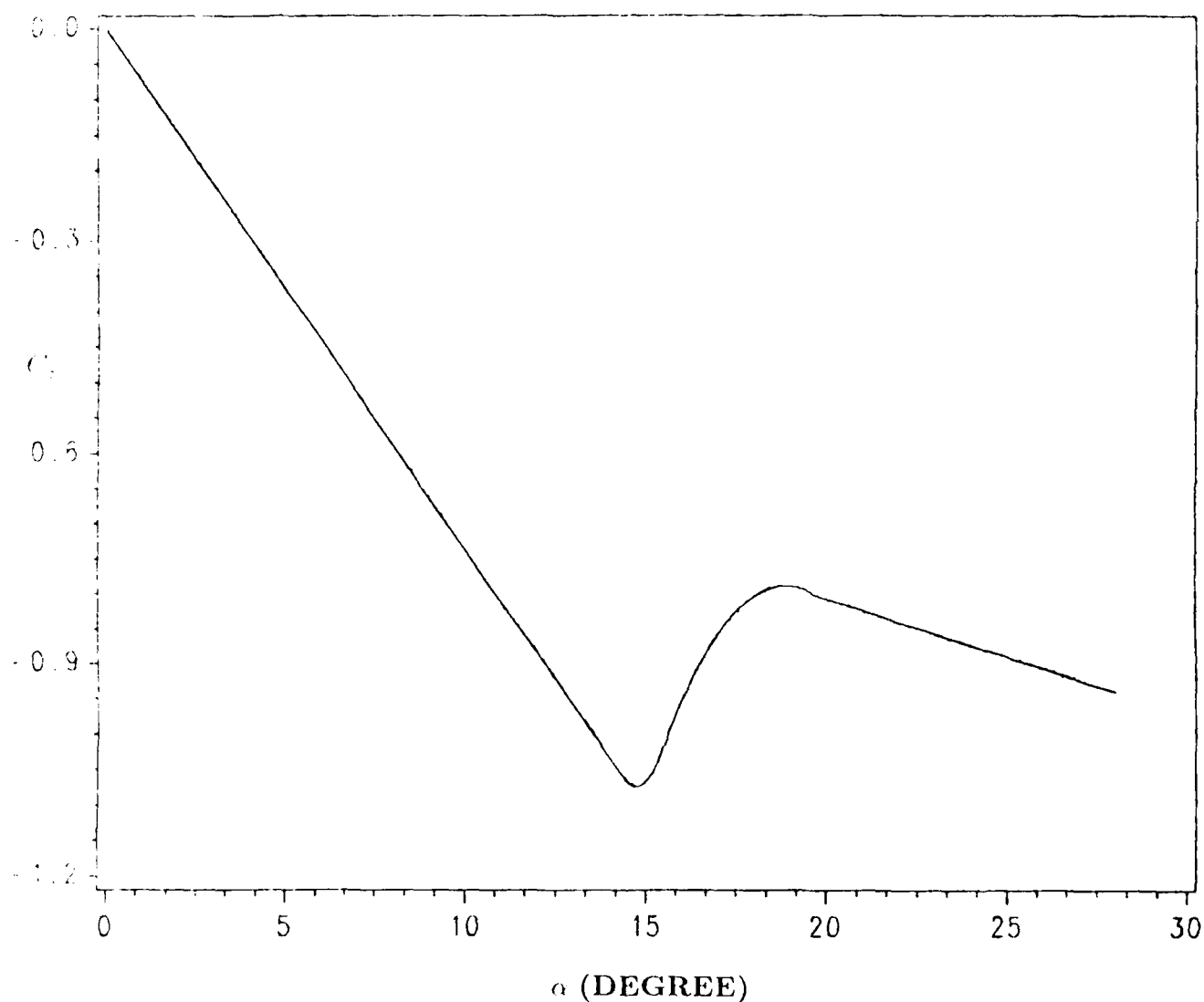
$$C_z(\alpha) = -0.07378494\alpha, \quad \alpha \leq 14.36^\circ. \quad (3.3)$$

In the stall region between 14.36° and 15.6° the C_z curve is quadratic in nature and is represented accurately by the quadratic equation

$$C_z(\alpha) = 0.09722\alpha^2 - 2.8653\alpha + 20.03846, \quad 14.36^\circ \leq \alpha \leq 15.6^\circ. \quad (3.4)$$

In the stall/post-stall region between 15.6° and 19.6° the C_z curve reverses its curvature and is represented accurately by the quadratic equation

$$C_z(\alpha) = -0.01971\alpha^2 + 0.74391\alpha - 7.80753, \quad 15.6^\circ \leq \alpha \leq 19.6^\circ \quad (3.5)$$



REGION I: $\alpha \leq 14.36^\circ$, $C_z(\alpha) \simeq$ LINEAR FUNCTION

REGION II: $14.36^\circ \leq \alpha \leq 15.6^\circ$, $C_z(\alpha) \simeq$ QUADRATIC FUNCTION

REGION III: $15.6^\circ \leq \alpha \leq 19.6^\circ$, $C_z(\alpha) \simeq$ QUADRATIC FUNCTION

REGION IV: $19.6^\circ \leq \alpha \leq 28^\circ$, $C_z(\alpha) \simeq$ LINEAR FUNCTION

**FIGURE 3-1. NONLINEAR PLUNGING FORCE COEFFICIENT $C_z(\alpha)$
FOR T-2C AIRPLANE $\delta_e = -18^\circ$.**

In the post-stall region between 19.6° and 28° , the C_z curve exhibits linear behavior

$$C_z(\alpha) = -0.01667\alpha - 0.47333, \quad 19.6^\circ \leq \alpha \leq 28^\circ. \quad (3.6)$$

The above division of the α interval into four α subspaces leads to an accurate representation of the nonlinear function $C_z(\alpha)$ by four low-order equations.

In each of the subspace regions described by Equations (3.3) through (3.6) an equilibrium point is chosen and the solution of the differential equation is approximated by the first three terms of its Volterra series. For simulation and analysis purposes, we use the differential equation form for the Volterra series terms. Following the procedure outlined in Section 2, with state $x = [\alpha, q]^T$ and input $u = \delta_e$ (elevator angle), we consider inputs of the form

$$\delta_e = \delta_{e_0} + k\delta_{e_1} \quad (3.7)$$

where δ_{e_0} is the equilibrium input and k is a real parameter needed for the perturbation analysis below and does not have physical significance. The solution to the nonlinear differential equations (3.1) and (3.2) has the form

$$x = x_0 + kx_1 + k^2x_2 + k^3x_3 + \dots \quad (3.8)$$

where $x_0 = [\alpha_0, q_0]^T$ is the equilibrium state and $x_i = [\alpha_i, q_i]^T$ is the contribution to the state from the i th term in the Volterra series. Substituting (3.7) and (3.8) into (3.1) and (3.2), expanding in a Taylor series with respect to k , and equating coefficients of equal powers of k results in differential equations for the first three Volterra series terms of the form

$$\begin{aligned} \dot{x}_1 &= Ax_1 + b\delta_{e_1} \\ \dot{x}_2 &= Ax_2 + g_1(x_1), \quad x_2(0) = 0 \\ \dot{x}_3 &= Ax_3 + g_2(x_1, x_2), \quad x_3(0) = 0. \end{aligned} \quad (3.9)$$

In all four subspaces regions the column matrix b is given by (see Appendix C for Region II)

$$b = \begin{bmatrix} -1.8336 \\ -8.595 \end{bmatrix} \quad (3.10)$$

and the matrix A , the Jacobian at $(\alpha_0, q_0, \delta_{e_0})$, has the form

$$A = \begin{bmatrix} A_{11} & 1 \\ -5.73 & 0 \end{bmatrix} \quad (3.11)$$

The entry A_{11} depends in this example on the value α_0 . However, in subspace regions I and IV, as described by equations (3.3) and (3.6), the approximation (3.9) is linear with $g_1(x_1) = g_2(x_1, x_2) = 0$ and A_{11} is independent of α_0 with values -0.67646 and -0.152831 , respectively.

In the subspace regions II and III, as described by Equations (3.4) and (3.5), the functions g_1 and g_2 have the form

$$g_1(x_1) = \begin{bmatrix} g_{11}\alpha_1^2 \\ 0 \end{bmatrix} \quad (3.12)$$

$$g_2(x_1, x_2) = \begin{bmatrix} g_{21}\alpha_1\alpha_2 \\ 0 \end{bmatrix} \quad (3.13)$$

where the constants g_{11} and g_{21} depend on the particular region. We picked the equilibrium point for each region by first assigning a value for δ_{e_0} and then calculating α_0, q_0 from equations (3.1) and (3.2). In region II, the Volterra series has been expanded about the equilibrium point $(\alpha_0, q_0, \delta_{e_0}) = (14.36^\circ, -1.7552^\circ/sec, -9.24^\circ)$ giving $g_{11} = 0.8913, g_{21} = 1.826$ and $A_{11} = -0.6709$. In region III, the Volterra series has been expanded about the equilibrium point $(\alpha_0, q_0, \delta_{e_0}) = (17.6^\circ, -7.911239^\circ/sec, -11.4^\circ)$ giving $g_{11} = -0.180701, g_{21} = -0.361403$ and $A_{11} = 0.459482$. The calculations for g_{11}, g_{21} and A_{11} for region II are given in Appendix C. In the prediction analysis we use the following procedure. Starting from conditions $\alpha^0 = 11^\circ, q^0 = 0$ and δ_e equal to a constant value, the Volterra model of the first subspace describes the airplane's response until $\alpha = 14.36^\circ$ is reached. At this point the Volterra model of the second subspace describes the response until α reaches one of the boundaries, 14.36° or 15.6° . If the response intersects the 14.36° boundary, then the first Volterra model governs the response. If the response intersects the 15.5° boundary, then the third subspace model governs the motion while α remains between 15.6° and 19.6° . The fourth subspace model governs the model when α is between 19.6° and 28° . Upon entering a new region, the equilibrium state, x_0 , is changed to correspond to the equilibrium point

used in this region. The initial linear state x_1 is set equal to $x - x_0$, the value of the state at the boundary crossing minus the new equilibrium value. The initial "nonlinear" states, x_2, x_3, \dots , are set equal to zero.

We define \hat{x}_j as the state resulting from a Volterra approximation with j terms

$$\hat{x}_j = x_0 + \sum_{i=1}^j x_i = \begin{bmatrix} \hat{\alpha}_j \\ \hat{q}_j \end{bmatrix} \quad (3.14)$$

where x_0 is the equilibrium state.

In the example described above we have $j = 3$

$$\hat{x}_3(t) = x_0 + x_1(t) + x_2(t) + x_3(t) \quad (3.15)$$

where $x_i(t), i = 1, 2, 3$ satisfies (3.9). The solution to the nonlinear differential equations (3.1) and (3.2) is denoted by $x(t) = [\alpha(t), q(t)]^T$. We use a fourth-order Runge-Kutta routine to calculate $x(t)$, thus $\alpha(t)$.

We consider two step inputs $\delta_e = -9.2^\circ$ and $\delta_e = -9.4^\circ$. The onset of the limit cycle occurs between these two inputs. For $\delta_e = -9.2^\circ$, the responses $\alpha(t)$ and $\hat{\alpha}_3(t)$ are compared in Figure 3-3. Their differences are presented by the solid line in Figure 3-6. We observe no limit cycle for this input. The three-term Volterra response is an excellent match to the nonlinear response. The maximum difference is only 0.05 degrees as shown in Figure 3-6.

For $\delta_e = -9.4^\circ$, the responses $\alpha(t)$ and $\hat{\alpha}_3(t)$ are compared in Figure 3-4 with their differences presented by the solid line in Figure 3-7. This input of $\delta_e = -9.4^\circ$ generates a limit cycle. Again the three-term Volterra model response is an excellent match with a maximum difference of 0.01 degrees over a time interval of 100 seconds as shown in Figure 3-7.

For comparison, we consider a piecewise-linear model, choosing the following regions and linearized models of $C_z(\alpha)$, Figure 3-2,

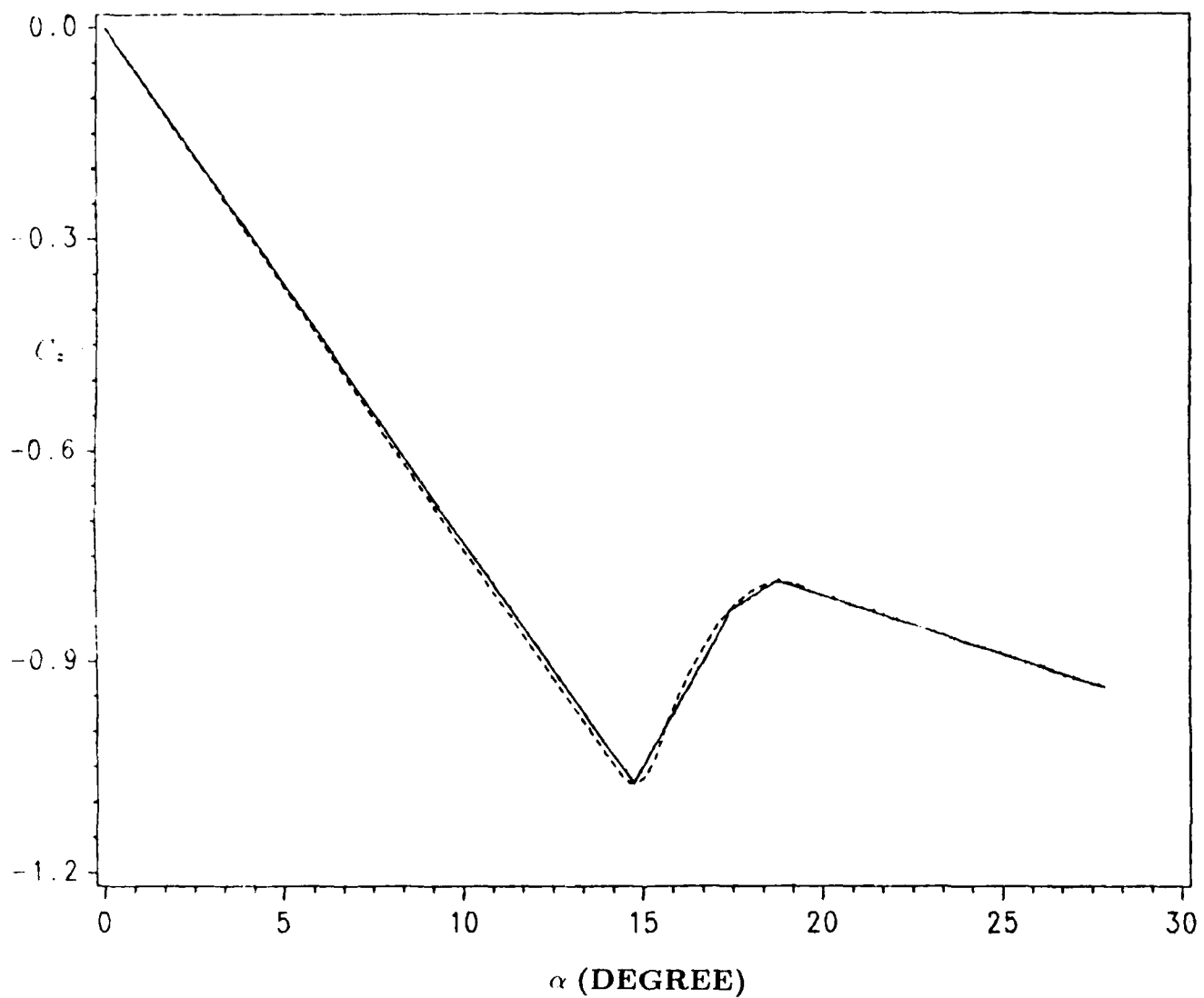
$$C_z(\alpha) = (-0.07281587)\alpha, \quad \alpha \leq 14.74^\circ \quad (3.16a)$$

$$C_z(\alpha) = -1.073305924 + 0.088470922(\alpha - 14.74^\circ), \quad 14.74^\circ < \alpha \leq 17.4^\circ \quad (3.16b)$$

$$C_z(\alpha) = -0.8308956 + 0.03309905(\alpha - 17.4^\circ), \quad 17.4^\circ < \alpha \leq 18.87^\circ \quad (3.16c)$$

$$C_z(\alpha) = -0.7882234 - 0.016633734(\alpha - 18.87^\circ), \quad 18.87^\circ < \alpha \leq 28^\circ \quad (3.16d)$$

The responses using the above approximations are compared with the nonlinear responses, $\alpha(t)$, in Figure 3-5. The differences are presented by the broken line in Figure 3-6 for $\delta_e = -9.2^\circ$, and in Figure 3-7, for $\delta_e = -9.4^\circ$. The maximum difference in Figure 3-6 is about 2.5 degrees, and in Figure 3-7, about 0.7 degrees. These differences are one to two orders of magnitude more than those obtained using the Volterra approximation.



REGION I: $\alpha \leq 14.74^\circ$

REGION II: $14.74^\circ \leq \alpha \leq 17.4^\circ$

REGION III: $17.4^\circ \leq \alpha \leq 18.87^\circ$

REGION IV: $18.87^\circ \leq \alpha \leq 28^\circ$

FIGURE 3-2. PIECEWISE-LINEAR FIT (SOLID LINE) FOR $C_z(\alpha)$ CURVE (BROKEN LINE).

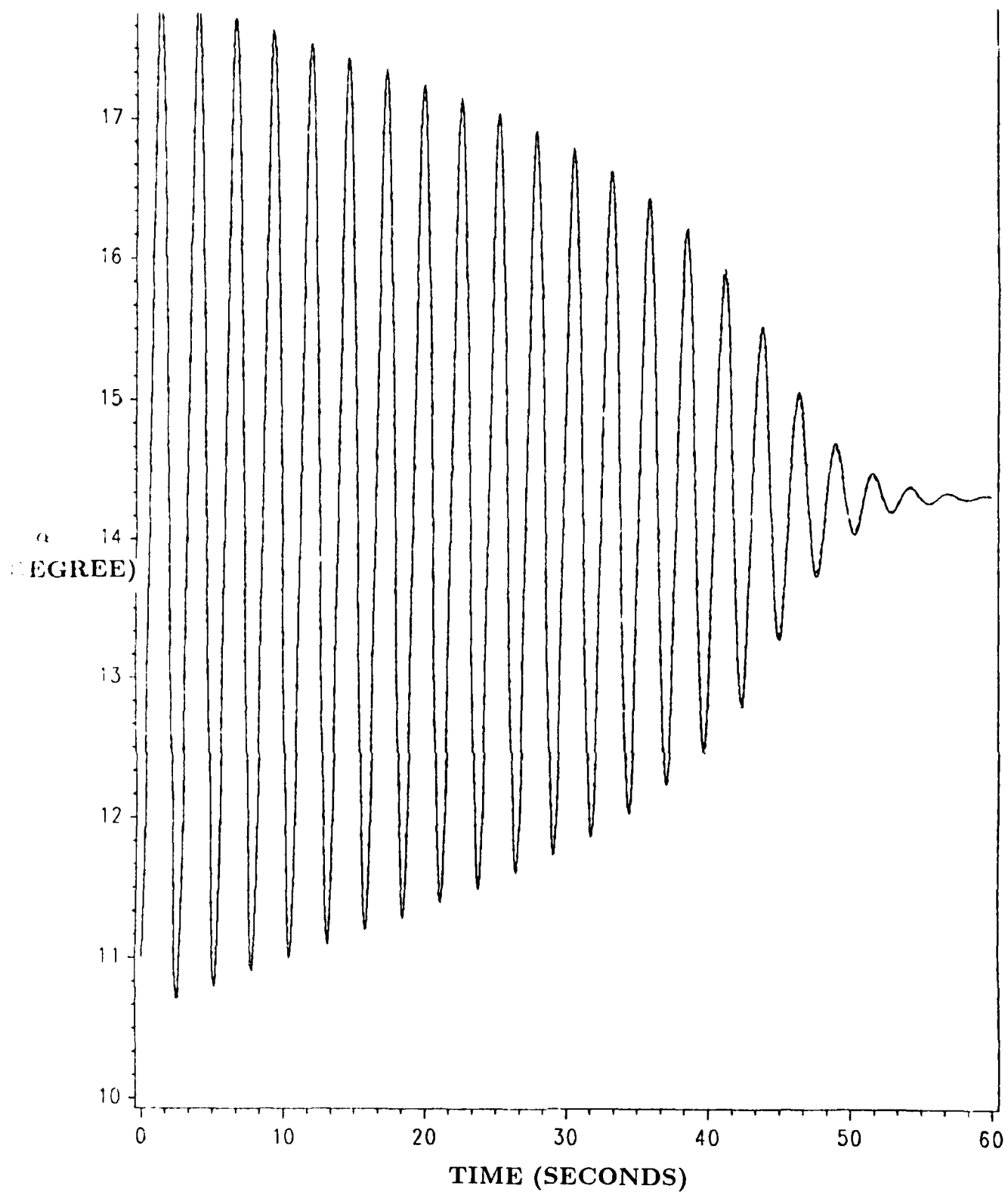


FIGURE 3-3. THREE-TERM VOLTERRA RESPONSE (BROKEN LINE) PROVIDES EXCELLENT APPROXIMATION FOR NONLINEAR SYSTEM RESPONSE (SOLID LINE) FOR $\delta_e = -9.2^\circ$, $\alpha^0 = 11^\circ$ AND $q^0 = 0$.

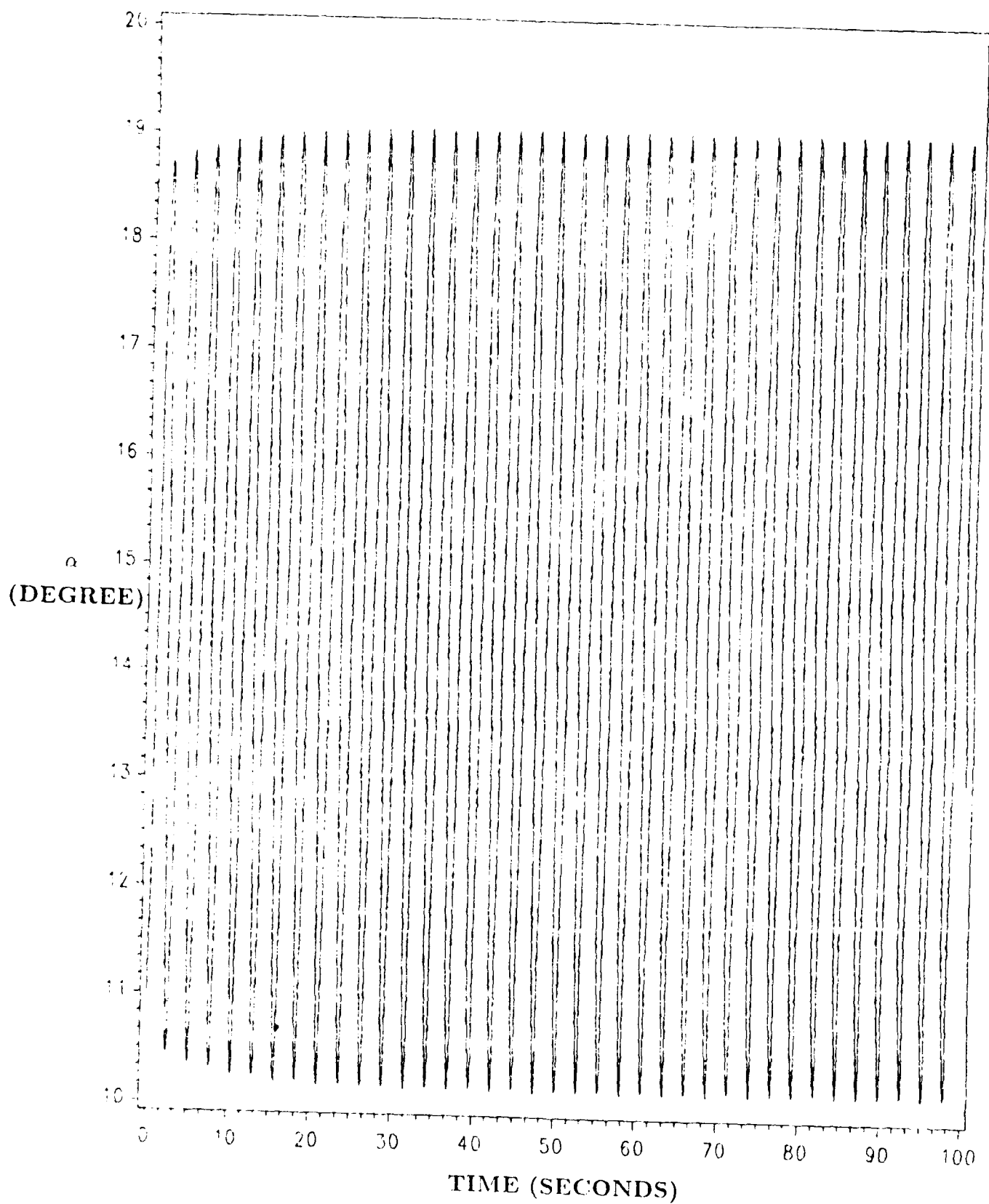


FIGURE 3-4. THREE-TERM VOLTERRA APPROXIMATION (BROKEN LINE) PREDICTS NONLINEAR SYSTEM (SOLID LINE) LIMIT CYCLE FOR $\delta_e = -9.4^\circ$, $\alpha^0 = 11^\circ$ AND $q^0 = 0$.

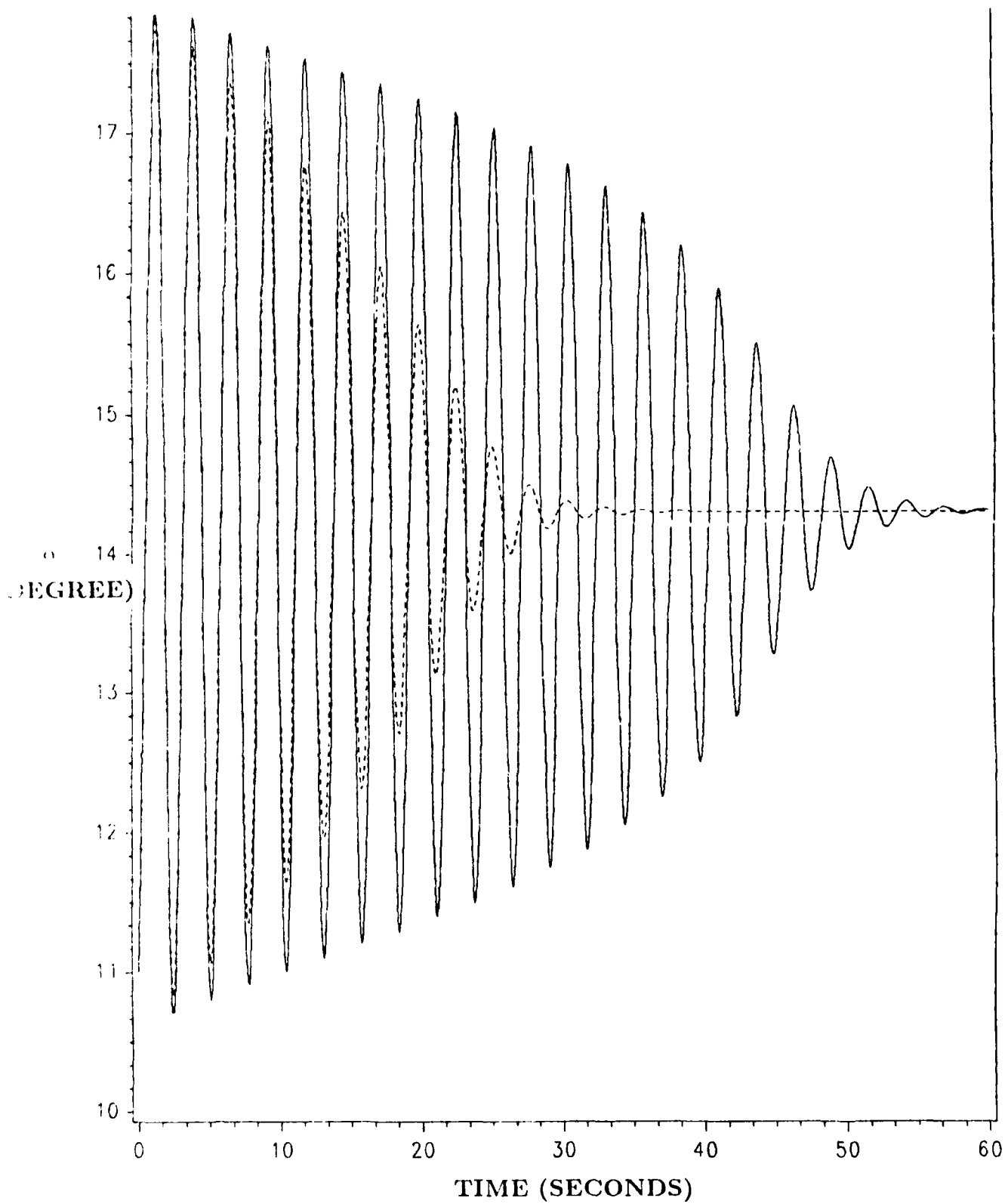


FIGURE 3-5. PIECEWISE-LINEAR RESPONSE (BROKEN LINE) FAILS TO MATCH NONLINEAR SYSTEM RESPONSE (SOLID LINE) FOR $\delta_e = -9.2^\circ$, $\alpha^0 = 11^\circ$ AND $q^0 = 0$.

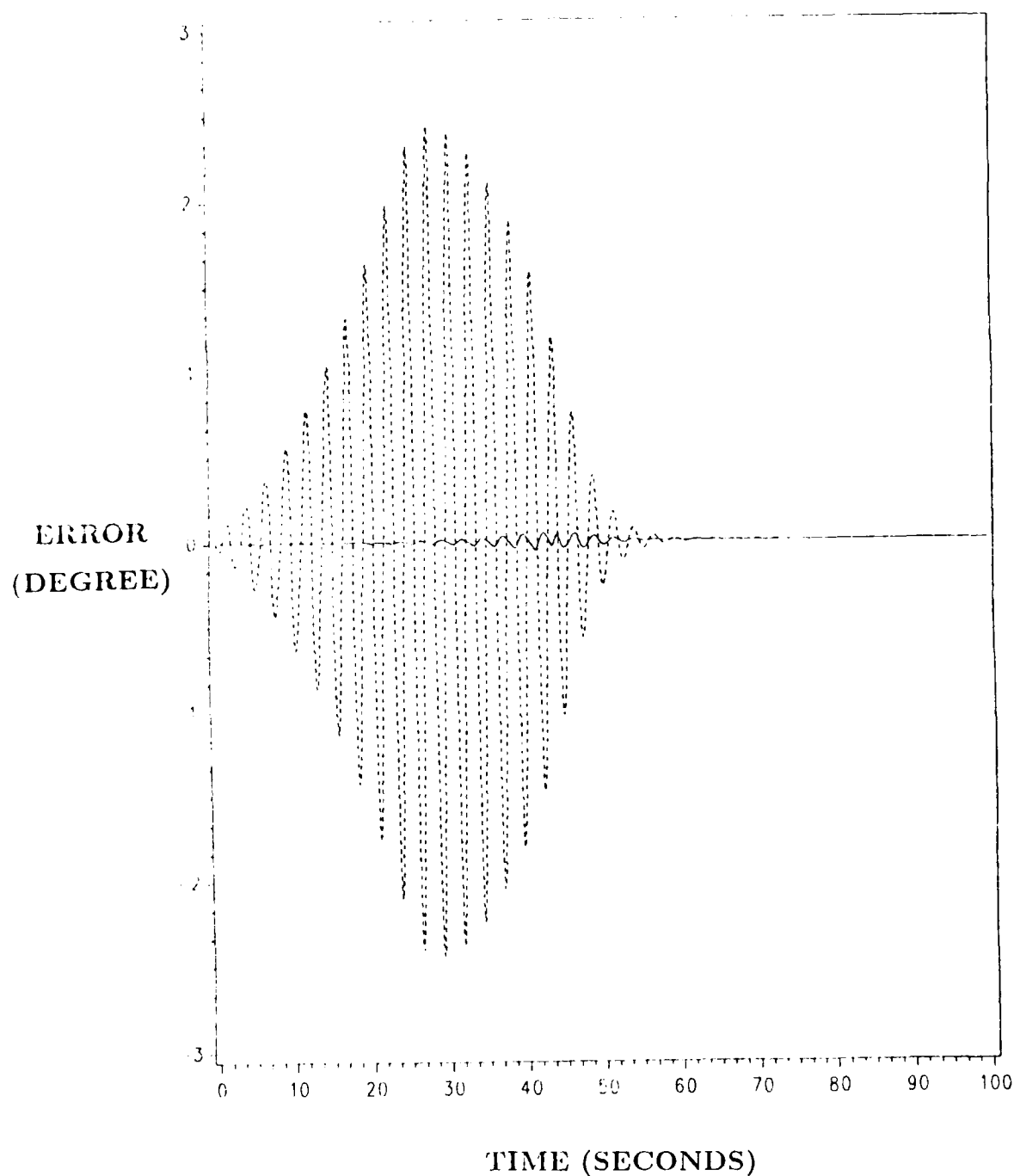


FIGURE 3-6. COMPARISON OF THREE-TERM VOLTERRA AND PIECEWISE LINEAR ERRORS FOR $\delta_e = -9.2^\circ$, $\alpha^0 = 11^\circ$ AND $q^0 = 0$. SOLID LINE REPRESENTS THE ERROR $\hat{\alpha}_3(t) - \alpha(t)$, BROKEN LINE REPRESENTS THE ERROR FOR THE PIECEWISE-LINEAR APPROXIMATION.

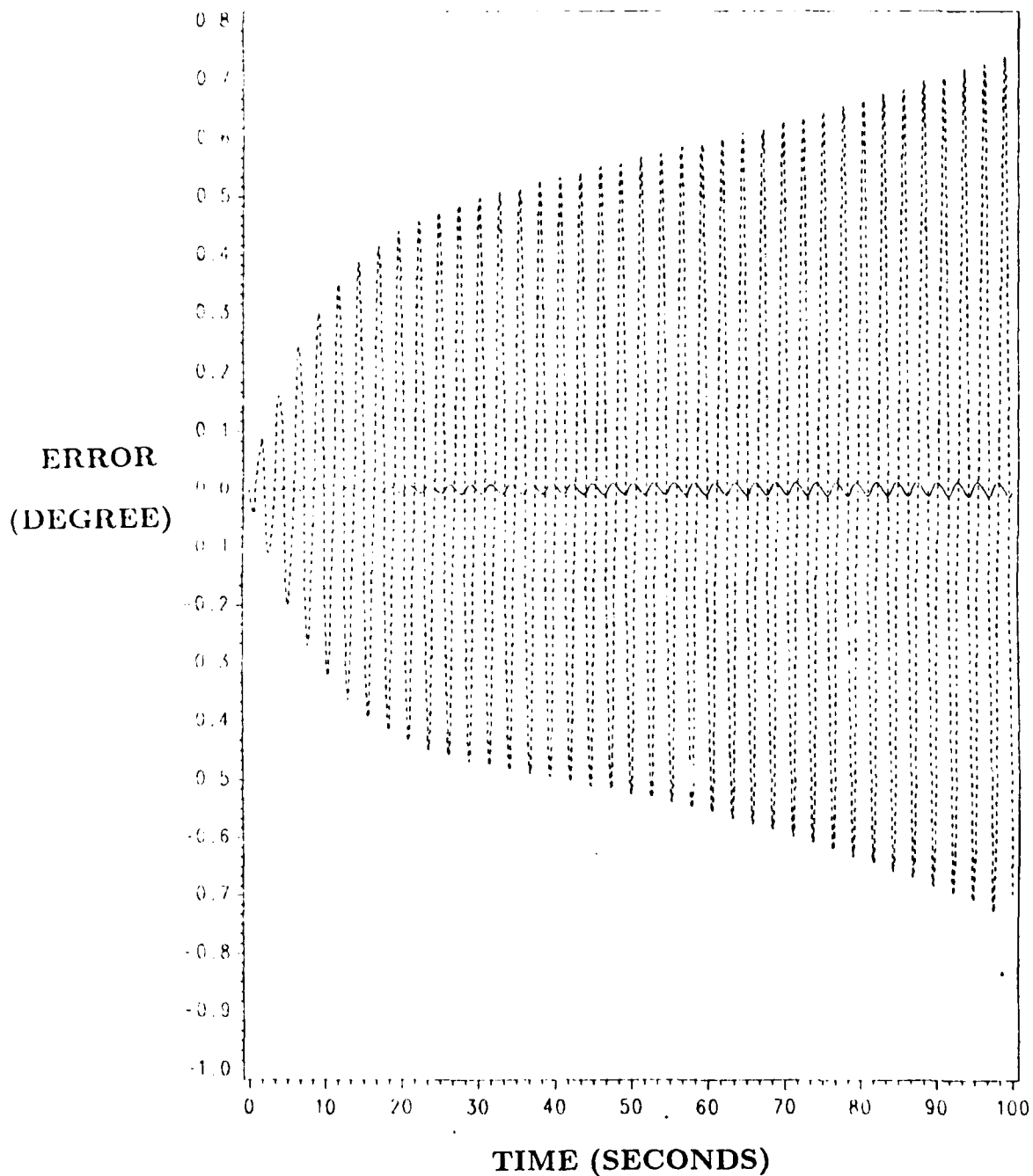


FIGURE 3-7. COMPARISON OF THREE-TERM VOLTERRA AND PIECEWISE-LINEAR ERRORS FOR $\delta_e = -9.4^\circ$, $\alpha^0 = 11^\circ$, AND $q^0 = 0$. SOLID LINE REPRESENTS THE ERROR $\hat{\alpha}_3(t) - \alpha(t)$. BROKEN LINE REPRESENTS THE ERROR FOR THE PIECEWISE-LINEAR APPROXIMATION.

3.2 Wing Rock Limit Cycle: Example 2

Unsteady aerodynamic effects at high α generate a wing rock limit cycle phenomenon on aircraft configurations incorporating slender forebodies (e.g., F-5 and X-29), Nguyen, et al [24, 26] and Brandon, et al [30]. We consider a mathematical model of an experimental wind-tunnel wing rock model developed by NASA Langley Research Center, Nguyen, Whipple and Brandon [24]. The following equations (3.17) and (3.18) hold for a wind-tunnel sting mounted model on an apparatus which allows the model to rotate freely about its roll axis with no angular limitation.

$$\dot{\varphi} = p \quad (3.17)$$

$$\dot{p} = \frac{\bar{q}Sb}{I_x} \left[C_{l_\beta}(\alpha)\beta + \bar{C}_{l_p}(\alpha, \beta) \frac{pb}{2V} \right] \quad (3.18)$$

where φ and p are the roll angle in radians and roll rate in radians per second, respectively. Here, the constants \bar{q} , S , b , I_x and V are the dynamic pressure, wing reference area, wing span, roll moment of inertia and free stream air speed, respectively. The coefficient C_{l_β} is the rolling moment stability derivative due to sideslip β . The coefficient \bar{C}_{l_p} is the rolling moment derivative due to roll rate p and sideslip rate $\dot{\beta}$. Approximate wind-tunnel values of these coefficients are given by Nguyen, Whipple and Brandon for the angle of attack $\alpha = 30^\circ$. See the development in Appendix D.

$$C_{l_\beta}(\alpha = 30^\circ) = -0.4584 \quad (3.19)$$

$$\bar{C}_{l_p}(\alpha = 30^\circ, \beta) = 0.4[1 - 7.64|\beta|], \quad (3.20)$$

$$0 \leq |\beta| \leq 0.35$$

$$\varphi = 2\beta \quad (3.21)$$

Evaluating the constants in (3.18) we have, see [23],

$$\frac{1}{2} \left(\frac{\bar{q}Sb}{I_x} \right) C_{l_\beta}(\alpha = 30^\circ) = -26.6667 \quad (3.22)$$

$$\left(\frac{\bar{q}Sb}{I_x} \right) \left(\frac{b}{2V} \right) \bar{C}_{l_p}(\alpha = 30^\circ, \varphi) = 0.76485[1 - 3.82|\varphi|] \quad (3.23)$$

In view of (3.22) and (3.23), Equation (3.18) becomes

$$\dot{p} = -26.6667\varphi + 0.76485[1 - 3.82|\varphi|]p \quad (3.21)$$

Our nonlinear model is described by (3.17) and (3.24).

The nonlinear equation (3.24) lends itself to separation into two regions: Region I with $\varphi \geq 0$ and Region II with $\varphi < 0$.

$$\dot{p} = -26.6667\varphi + 0.76485[1 + (-1)^j 3.82\varphi]p \quad (3.25)$$

where j denotes the region.

Let $x = [\varphi, p]^T$ be the state of the nonlinear equations (3.17) and (3.24). Let $x_i = [\varphi_i, p_i]^T$ be the contribution to the state from the i th term in the Volterra series. The differential equations for the five-term Volterra series approximation have the form

$$\dot{x}_1 = Ax_1 \quad (3.26a)$$

$$\dot{x}_2 = Ax_2 + g_1(x_1), \quad x_2(0) = 0 \quad (3.26b)$$

$$\dot{x}_3 = Ax_3 + g_2(x_1, x_2), \quad x_3(0) = 0 \quad (3.26c)$$

$$\dot{x}_4 = Ax_4 + g_3(x_1, x_2, x_3), \quad x_4(0) = 0 \quad (3.26d)$$

$$\dot{x}_5 = Ax_5 + g_4(x_1, x_2, x_3, x_4), \quad x_5(0) = 0. \quad (3.26e)$$

The equilibrium point of (3.17) and (3.24) is $\varphi_0 = 0$, $p_0 = 0$. The A matrix in (3.26) is given by

$$A = \begin{bmatrix} 0 & 1 \\ -26.6667 & 0.76485 \end{bmatrix}. \quad (3.27)$$

The g_i functions in (3.26) have the form

$$g_i(x_1, \dots, x_i) = \begin{bmatrix} 0 \\ (-1)^j 2.92192 g_{i2}(x_1, \dots, x_i) \end{bmatrix} \quad (3.28a)$$

where j denotes the region ($j = 1$ or $j = 2$) and where

$$g_{12}(x_1) = \varphi_1 p_1 \quad (3.28b)$$

$$g_{22}(x_1, x_2) = \varphi_1 p_2 + \varphi_2 p_1 \quad (3.28c)$$

$$g_{32}(x_1, x_2, x_3) = \varphi_1 p_3 + \varphi_2 p_2 + \varphi_3 p_1 \quad (3.28d)$$

$$g_{42}(x_1, x_2, x_3, x_4) = \varphi_1 p_4 + \varphi_2 p_3 + \varphi_3 p_2 + \varphi_4 p_1 \quad (3.28e)$$

As in eq. (3.14), we let \hat{x}_j be the state resulting from a Volterra series with j terms. For $j = 1, 2, \dots, 5$, the roll angle responses for the initial condition $\varphi(0) = 5.73^\circ$ and $p(0) = 0.0$ are presented in Figures 3-8 through 3-12 respectively. The roll-angle response of the linearized system $\dot{x}_1 = Ax_1$ is compared with the nonlinear response in Figure 3-8. The linearized system diverges to a roll angle of 180° after 9 seconds; it does not predict the stable limit cycle. The limit cycle is predicted by the two-term Volterra approximation; the amplitude is short by about 7 degrees. The three-term Volterra approximation overpredicts the amplitude by about 5 degrees. The four-term and five-term Volterra approximations provide good predictions for both the amplitude and the period of the wing rock limit cycle, Table 3.1. The five-term Volterra approximation predicts the amplitude to within 0.31 degrees. The nonlinear system response was calculated using a fourth-order Runge-Kutta routine.

3.1. Comparison of Predicted Wing Rock Limit Cycle Characteristics

System	φ , Roll Angle	
Volterra Approximation	Period (Seconds)	Amplitude (Degrees)
two-Terms	1.2100	28.15
three-Terms	1.2257	40.60
four-Terms	1.21500	34.46
five-Terms	1.21857	35.65
Nonlinear System	1.2187	35.34

We observe that both the period and amplitude values for the Volterra approximations given in Table 3.1 approach the corresponding value for the nonlinear system. Let $E_i, i = 2, 3, 4, 5$ denote the error for the amplitude as predicted by the i -term Volterra approximation.

It follows that

$$\frac{|E_{i+1}|}{|E_i^2|} \leq .4, \quad i = 2, 3, 4.$$

Thus we might suspect quadratic convergence for the sequence $\{E_i\}_{i=1}^{\infty}$. We make this observation for this one example only and note that it is based on numerical results for four terms.

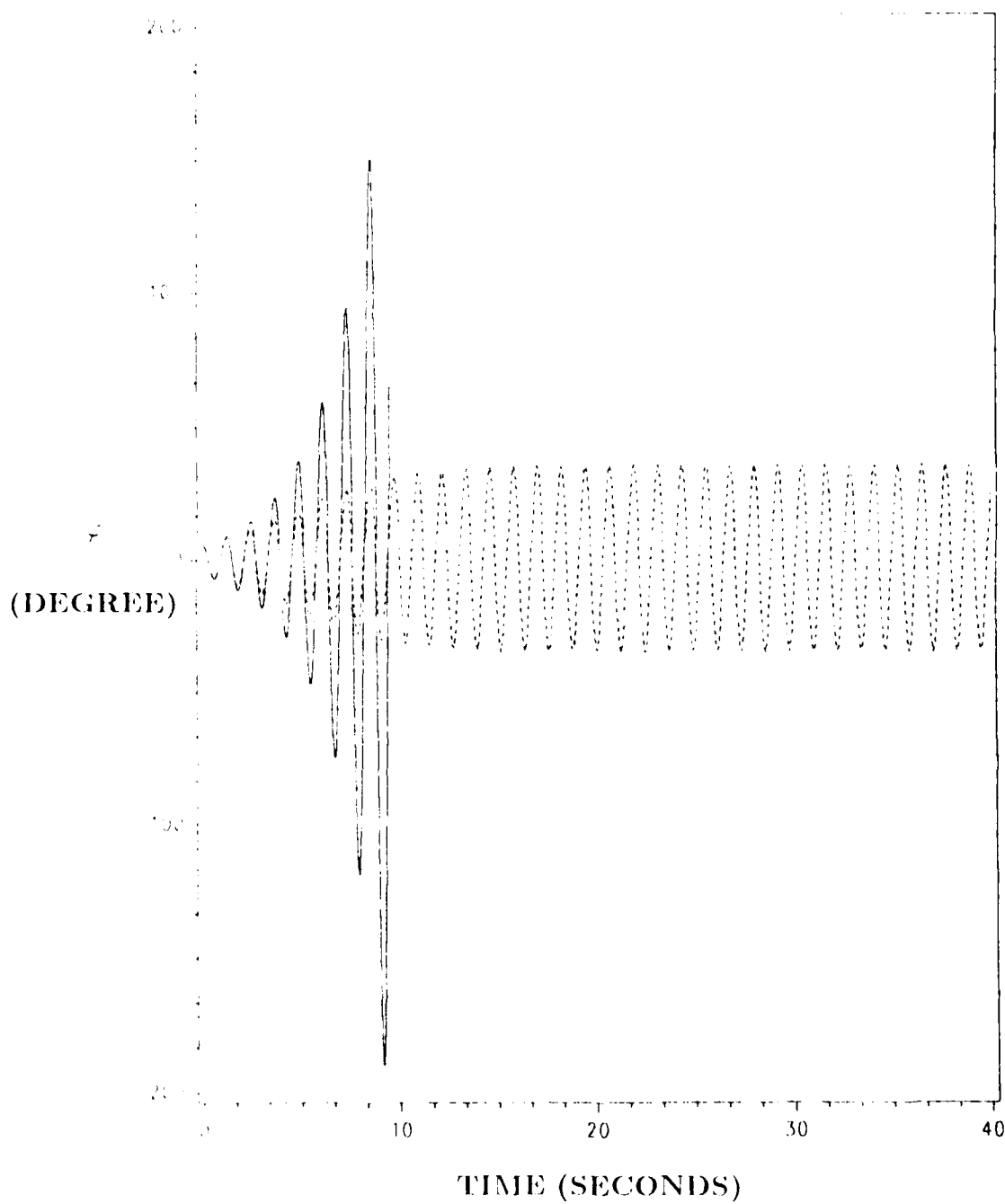


FIGURE 3-8. LINEARIZED SYSTEM (SOLID LINE) DIVERGES, FAILING TO PREDICT STABLE WING ROCK OF NONLINEAR SYSTEM WITH $\varphi^0 = 5.73^\circ$, $p^0 = 0$.

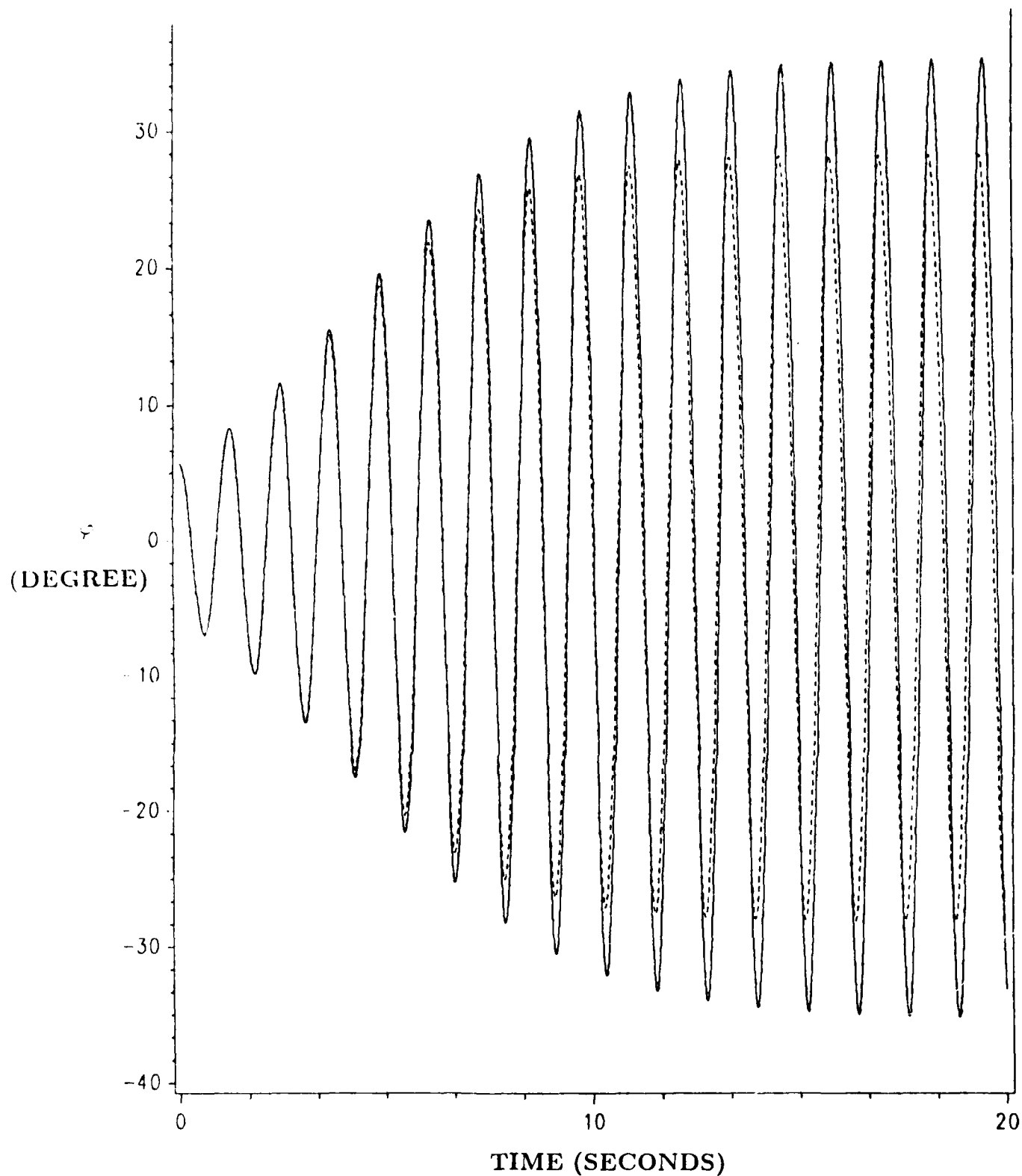


FIGURE 3-9. TWO-TERM VOLTERRA APPROXIMATION (BROKEN LINE) PREDICTS STABLE WING ROCK OF NONLINEAR SYSTEM (SOLID LINE) FOR $\varphi^0 = 5.73, p^0 = 0$ WITH 7.2° AMPLITUDE ERROR.

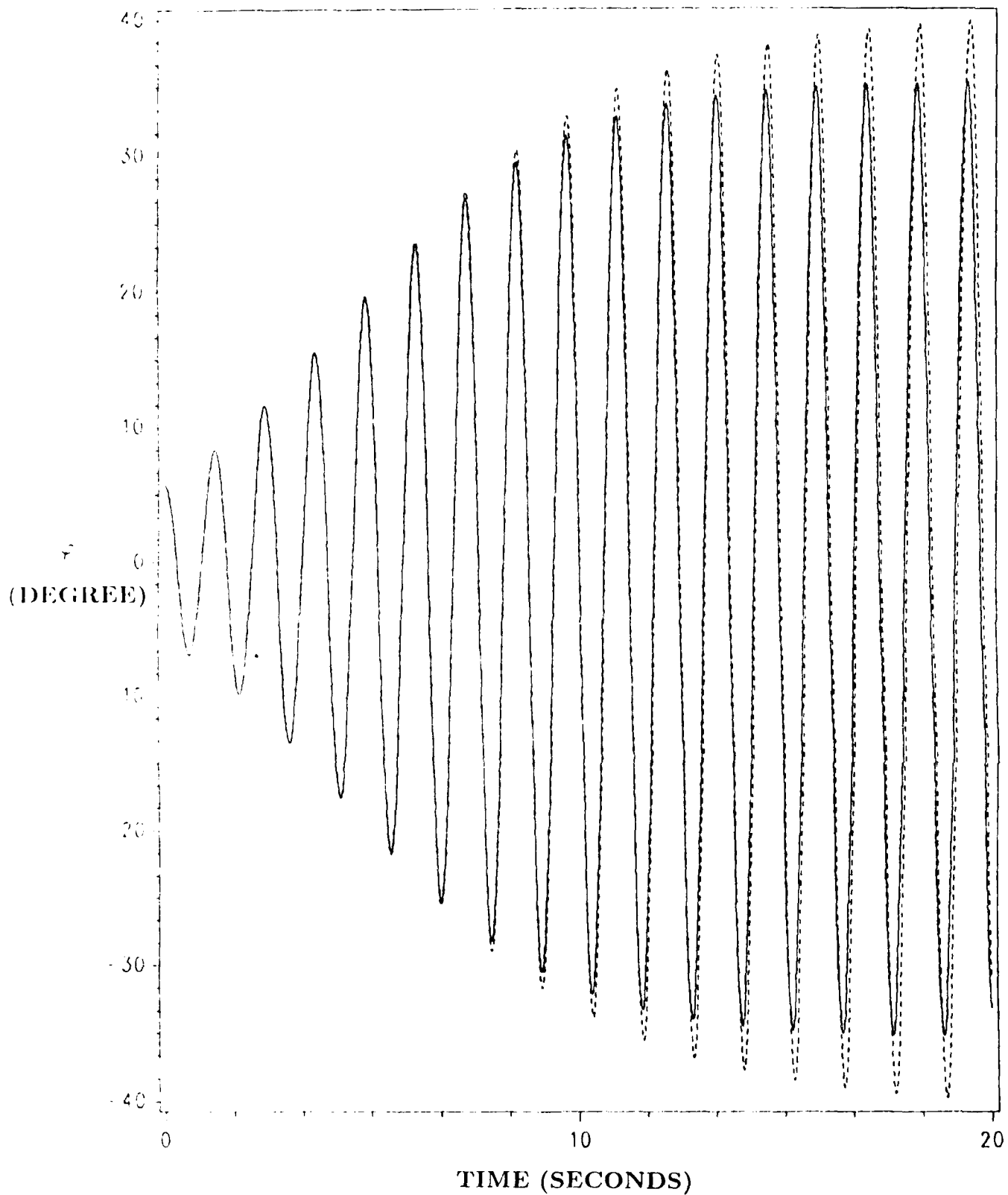


FIGURE 3-10. THREE-TERM VOLTERRA APPROXIMATION (BROKEN LINES) PREDICTS STABLE WING ROCK OF NONLINEAR SYSTEM (SOLID LINE) FOR $\varphi^0 = 5.73$, $p^0 = 0$ WITH 5.26° AMPLITUDE ERROR.

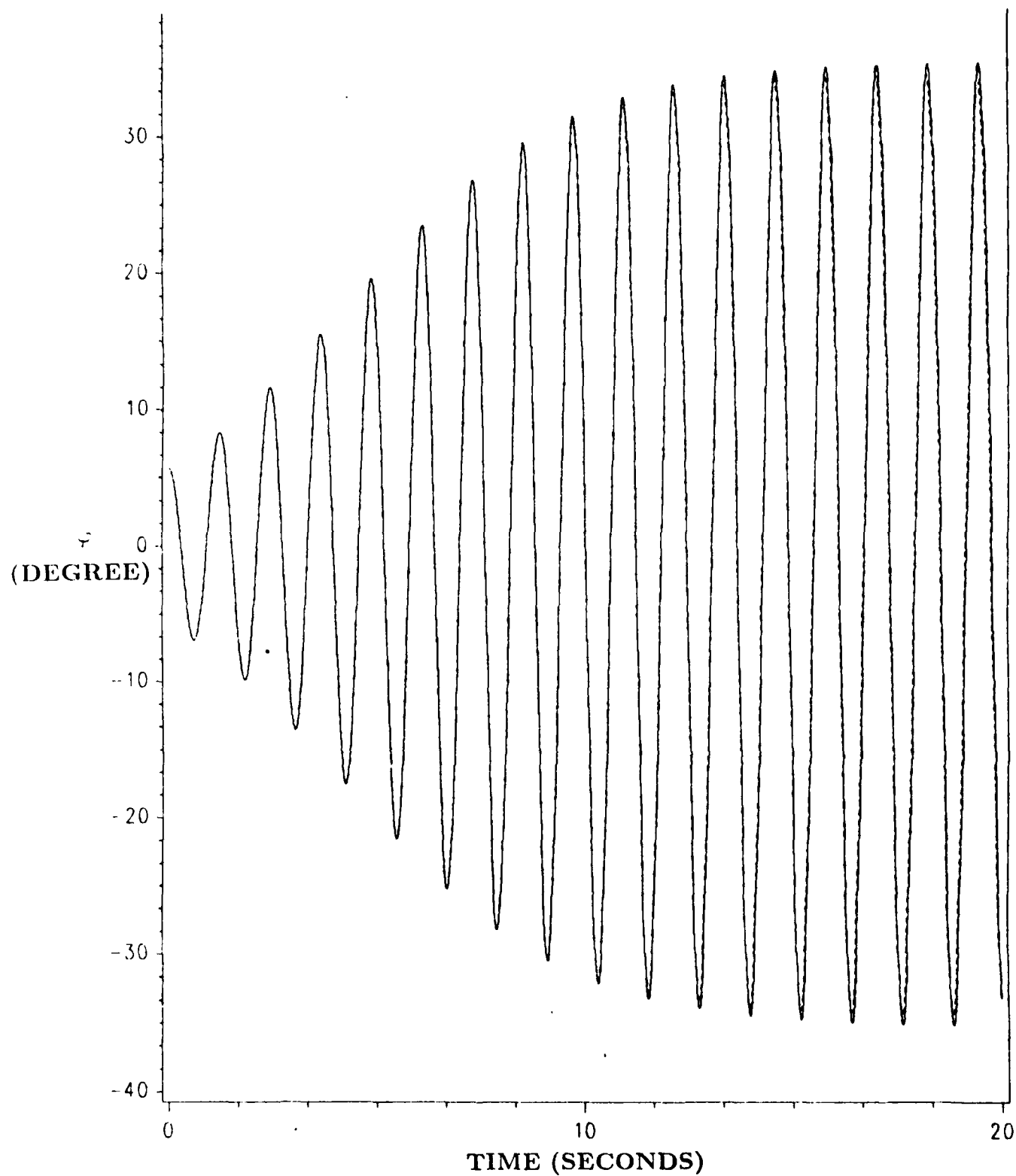


FIGURE 3-11. FOUR-TERM VOLTERRA APPROXIMATION (BROKEN LINE) PREDICTS STABLE WING ROCK OF NONLINEAR SYSTEM (SOLID LINE) FOR $\varphi^0 = 5.73, p^0 = 0$ WITH 0.9° AMPLITUDE ERROR.

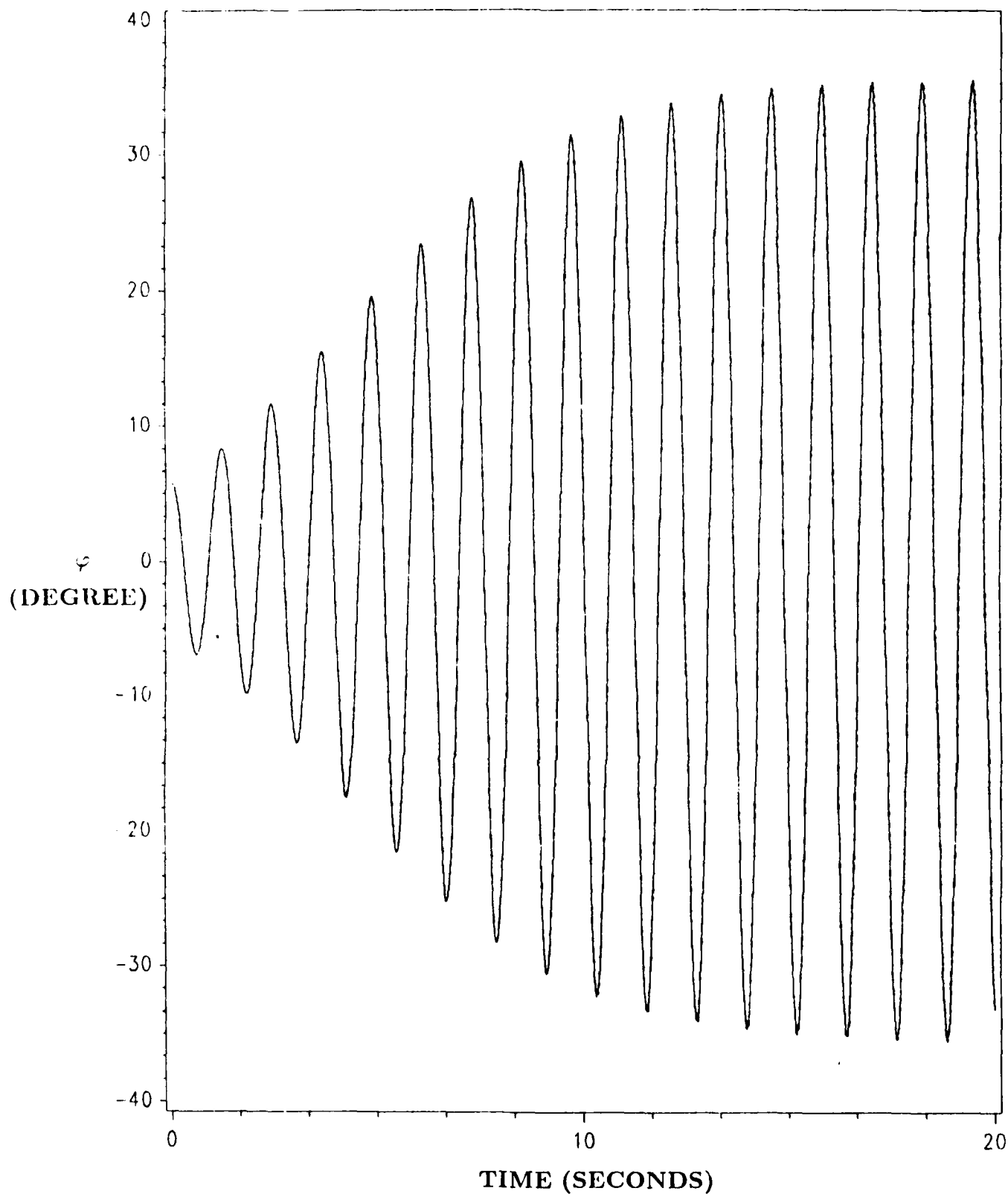


FIGURE 3-12. FIVE-TERM VOLTERRA APPROXIMATION (BROKEN LINE) PREDICTS STABLE WING ROCK OF NONLINEAR SYSTEM (SOLID LINE) FOR $\varphi^0 = 5.73, p^0 = 0$ WITH 0.31° AMPLITUDE ERROR.

4. Analysis

In this section we consider several approaches to analyzing the nonlinear limit cycles considered in Section 3. First we suggest an approach for analyzing the wing rock limit cycle that is based on the Volterra submodels developed previously. Following this, the usefulness of classical approaches to the analysis of the wing rock and longitudinal limit cycles is explored.

4.1 Volterra Series Analysis

In this section we apply the Volterra series subspace technique to the wing rock example given in Section 3.2. In particular, we obtain a two-term representation for the solution of the system

$$\dot{\varphi} = p \quad (4.1)$$

$$\dot{p} = -26.67\varphi + 0.76485[1 - 3.82|\varphi|]p$$

For convenience we let $a = 26.67$, $b = 0.76485$, $c = 3.82b$ and define the 2×2 matrix A by

$$A = \begin{bmatrix} 0 & 1 \\ -a & b \end{bmatrix}.$$

The system (4.1) can now be represented by the matrix equation

$$\dot{x} = Ax + g(x) \quad (4.2)$$

where $x = [\varphi, p]^T$ and the nonlinear vector valued function g is defined by $g(x) = [0, -c|\varphi|p]^T$. It is to be noted that the unique equilibrium point for (4.2) is $x_0 = 0$. We assume that system (4.2) has a solution of the form $x = kx_1 + k^2x_2 + \dots$ where k is a constant and $x_i = [x_{i1}, x_{i2}]^T = [\phi_i, p_i]^T$, $i = 1, 2, \dots$. Substituting x into (4.2) yields

$$k\dot{x}_1 + k^2\dot{x}_2 + \dots = A(kx_1 + k^2x_2 + \dots) + \begin{bmatrix} 0 \\ -c(kx_{11} + k^2x_{21} + \dots)(kx_{12} + k^2x_{22} + \dots) \end{bmatrix}$$

in the region $\varphi \geq 0$. At this point we equate the coefficients of the first and second powers of the constant k to obtain the following equations for the first and second terms of the

Volterra series representation

$$\dot{x}_1 = Ax_1 \quad (4.3)$$

and

$$\dot{x}_2 = Ax_2 + g_1(x_1) \quad (4.4)$$

where $g_1(x_1) = [0, -cx_{11}x_{12}]^T$. To include initial conditions, say $x(0) = x^0$, in system (4.2) we modify (4.3) through (4.4) to become

$$\dot{x}_1 = Ax_1, \quad x_1(0) = x^0 \quad (4.5)$$

and

$$\dot{x}_2 = Ax_2 + g_1(x_1), \quad x_2(0) = 0 \quad (4.6)$$

The state transition matrix for (4.5) is given by (see Appendix F)

$$e^{At} = e^{bt/2} \begin{bmatrix} B_{11}(t) & B_{12}(t) \\ B_{21}(t) & B_{22}(t) \end{bmatrix}$$

where

$$\begin{aligned} B_{11}(t) &= \cos\omega_0 t - \frac{b}{2\omega_0} \sin\omega_0 t, & B_{12}(t) &= \frac{1}{\omega_0} \sin\omega_0 t \\ B_{21}(t) &= \frac{-a}{\omega_0} \sin\omega_0 t, & B_{22}(t) &= \cos\omega_0 t + \frac{b}{2\omega_0} \sin\omega_0 t \end{aligned} \quad (4.7)$$

and $\omega_0 = \sqrt{(4a - b^2)/4}$. For $x^0 = [0, p^0]^T$ we have

$$x_1(t) = e^{At} \begin{bmatrix} 0 \\ p^0 \end{bmatrix} = p^0 e^{bt/2} \begin{bmatrix} B_{12}(t) \\ B_{22}(t) \end{bmatrix} \quad (4.8)$$

and

$$x_2(t) = e^{At} \cdot 0 + \int_0^t e^{A(t-\tau)} \begin{bmatrix} B_{12}(-\tau) \\ B_{22}(-\tau) \end{bmatrix} B_{12}(\tau) B_{22}(\tau) d\tau. \quad (4.9)$$

Using various integration techniques, we find that $x_2(t)$ has the form (see Appendix F)

$$\begin{aligned}
x_2(t) = & -c(p^0)^2 e^{At} \left\{ \left[\frac{-(3b^2 + 36\omega_0^2)}{-6ab} \right] \frac{\sin^3 \omega_0 t}{3\omega_0^3(b^2 + 36\omega_0^2)} e^{bt/2} \right. \\
& + \left[\frac{4b}{12a} \right] \frac{\sin^2 \omega_0 t \cos \omega_0 t}{\omega_0^2(b^2 + 36\omega_0^2)} e^{bt/2} \\
& + \left[\frac{-b^2 - 36\omega_0^2 + 24a}{(b^2 + 36\omega_0^2)a} \right] \frac{\cos \omega_0 t}{(b^2 + 36\omega_0^2)a} e^{bt/2} \\
& + \left[\frac{-8b^2}{b^3 + 36b\omega_0^2 - 24ab} \right] \frac{\sin \omega_0 t}{2a\omega_0(b^2 + 36\omega_0^2)} e^{bt/2} \\
& \left. + \left[\frac{-8b}{b^2 + 36\omega_0^2 - 24a} \right] \frac{1}{a(b^2 + 36\omega_0^2)} \right\}.
\end{aligned}$$

Combining (4.7), (4.8) and (4.10), we have a representation for the approximate solution $\hat{x}_2(t) = x_1(t) + x_2(t)$ for (4.1) with initial condition $\varphi(0) = 0, \dot{\varphi}(0) = p^0$. To calculate the amplitude and period for the limit cycle of the wing rock example, we can set

$$\hat{x}_2(t_1) = x_1(t_1) + x_2(t_1) = \begin{bmatrix} 0 \\ -p^0 \end{bmatrix} \quad (4.11)$$

where t_1 represents half the limit cycle period. Assuming that the limit cycle is symmetric with respect to the φ axis, equation (4.11) allows us to (at least in theory) solve for p^0 and t_1 in terms of a, b, c .

The exact representation for p^0 and t_1 in terms of the values a, b and c probably cannot be obtained in closed form, and ways to simplify the equations to obtain approximate solutions should be considered. From this example we see that simple (two-term) Volterra approximations lead to complicated expressions when solved explicitly. This indicates that techniques of a more qualitative and indirect nature may be needed to show how the explicit Volterra solutions can be simplified.

4.2 Classical Analysis

In this section we present several classical approaches to the analysis of the examples discussed in this report. A review of several standard techniques will serve to put the new approach we have considered into proper perspective and to suggest methods for carrying out analysis using Volterra submodels. In the following sections, the wing rock and longitudinal limit cycles are analyzed using an energy (Lyapunov) method, harmonic balance, and piecewise-linear analysis.

4.2.1 Wing Rock

The equation that described the wing rock considered in this report is of the form

$$\ddot{\varphi} + a\dot{\varphi} - b\dot{\varphi} + c|\varphi|\dot{\varphi} = 0 \quad (4.12)$$

where φ is the roll angle in radians and in our case $a = 26.7$, $b = 0.765$, and $c = 2.92$.

Most classical approaches to analysis of nonlinear dynamic behavior assume that the behavior is characterized by a single nonlinear differential equation (i.e. one region). Since this is the case with our simplified description of wing rock, it is an ideal candidate for application of classical methods.

Energy Analysis

A standard equation from mechanics, which involves nonlinear damping, is of the form, see [34],

$$\ddot{x} + h(x, \dot{x}) + g(x) = 0.$$

The energy of this system is given by

$$E = \dot{x}^2/2 + \int g(x)dx$$

and the change in energy with respect to time by

$$dE/dt = -\dot{x}h(x, \dot{x}).$$

Our equation (4-12) can be put in this form using the following correspondence

$$x = \varphi$$

$$g = a\varphi$$

$$h = -b\dot{\varphi} + c|\varphi|\dot{\varphi}.$$

To evaluate the change in energy of our system, we consider two cases.

- I. $\varphi > 0$: $-\dot{x}h(x, \dot{x}) = \dot{\varphi}^2[b - c\varphi]$
 $\Rightarrow dE/dt > (<)0$ when $\varphi < (>)b/c$
- II. $\varphi < 0$: $-\dot{x}h(x, \dot{x}) = \dot{\varphi}^2[b + c\varphi]$
 $\Rightarrow dE/dt > (<)0$ when $\varphi > (<)-b/c$

The regions of energy increase/decrease are shown in Figure 4-1. The situation shown in Figure 4-1 is similar to that of the classical Van der Pol oscillator. The origin is an unstable equilibrium point as the system energy increases in a neighborhood of the origin.

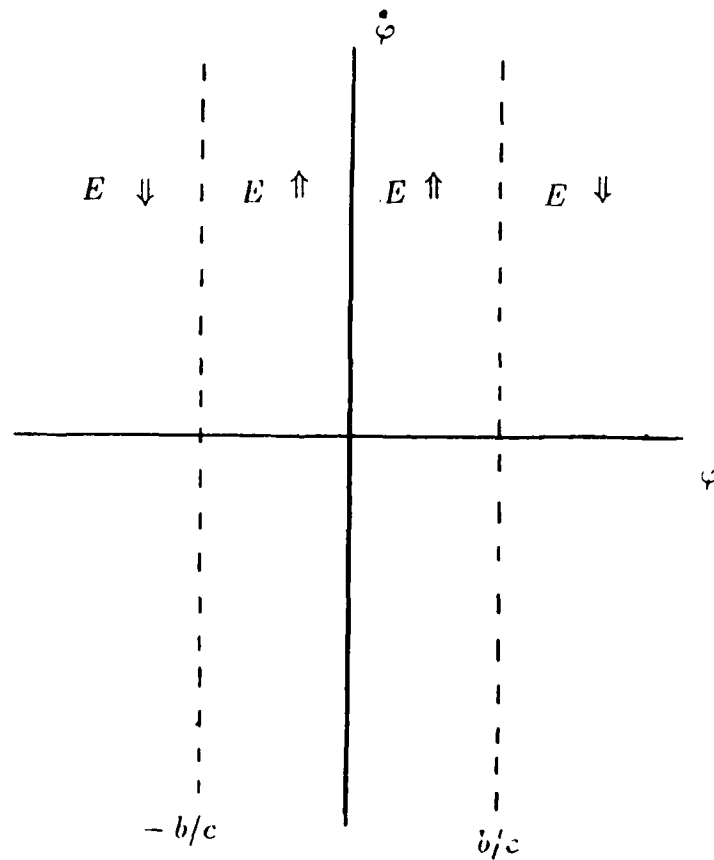


FIGURE 4-1. Regions of Energy Increase/Decrease

As the system energy increases, the system is forced into the region $|\varphi| > b/c$ where the energy is decreasing and in turn is forced back into the region $|\varphi| < b/c$ where the energy is increasing. This alternation between increasing and decreasing energy results in the observed limit cycle. If the coefficient of the nonlinear term, c , should change sign, then energy will increase everywhere in the phase plane and the system will be unstable.

This analysis also indicates why the linear submodel approach fails to predict a stable limit cycle. The linear submodels accurately reflect the behavior in a neighborhood of the origin, where the energy is always increasing, and thus predict completely unstable behavior. The Volterra submodels reflect the behavior over a larger region of the state space and somehow capture the positive damping that occurs for larger values of $|\phi|$. An area for future investigation would be to characterize the damping in a truncated Volterra approximation.

Although energy analysis is a very powerful tool for this second order example, its usefulness declines as the systems become more complicated. It is not generally possible to define a useful energy (Lyapunov) function for a complicated system of equations.

Harmonic Balance

To apply the first-order harmonic balance method, we assume that the oscillation is a pure sinusoid

$$\varphi = A \cos(wt) \quad (4-13)$$

of unknown amplitude and frequency. Substituting (4-13) into the original differential equation yields

$$-Aw^2 \cos(wt) + aA \cos(wt) + bAw \sin(wt) - cAw|A \cos(wt)| \sin(wt) = 0 \quad (4-14)$$

Substituting the Fourier series for $|\cos(wt)|$

$$|\cos(wt)| = \frac{2}{\pi} + \frac{4}{3\pi} \cos 2wt + \dots$$

into (4-14) and dropping all harmonics yields

$$-Aw^2 \cos(wt) + aA \cos(wt) + bAw \sin(wt) - \frac{2c}{\pi} A^2 w \sin(wt) - \frac{4}{6\pi} c A^2 w \sin(-wt) = 0$$

Equating the coefficients of the $\cos(\omega t)$ terms gives the equation for the limit cycle frequency

$$\omega = \sqrt{a}.$$

Equating the coefficients of the $\sin(\omega t)$ terms gives the equation for the limit cycle amplitude

$$A = \frac{3\pi b}{4c}.$$

Substituting the values of the parameters a, b, c for our case gives

$$\omega = 5.17 \quad (T = 1.216)$$

$$A = 35.37^\circ$$

which compare very favorably with the simulation results $T = 1.219$ and $A = 35.34^\circ$.

The harmonic balance method is a very powerful tool for analyzing simple oscillations and can be extended to higher order systems with a concomitant increase in complexity. In the next section we apply this technique to a more complicated example.

4.2.2 Longitudinal Limit Cycle

An important feature of the equations modeling the longitudinal limit cycle is that the nonlinearities cannot be represented in a simple manner over the entire range of interest. Most classical analysis techniques do not apply in this situation. The approach outlined in this report decomposes the state space into regions in which the nonlinearity can be represented by a low order polynomial. This section examines two other approaches.

The first approach approximates the nonlinearity by a piecewise-linear function and provides qualitative information about the behavior of the resulting system. The second approach represents the nonlinearity numerically, using a spline fit to wind tunnel data, and investigates the usefulness of harmonic balance techniques.

Piecewise Linear Analysis

We consider the longitudinal equations (3-1), (3-2) and the piecewise-linear approximation of $C_z(\alpha)$ given by (3-16). The system is unstable in regions II and III ($14.74^\circ < \alpha <$

18.87°), as the coefficient of α in $C_z(\alpha)$ is positive, and stable in regions I and IV. For a given constant input, δ_{e0} , the equilibrium value of α is found by setting $\dot{q} = 0$ and given by

$$\alpha_0 = 0.5 - 1.5\delta_{e0}.$$

For values of δ_{e0} between 0° and 9.5° , the equilibrium value of α is in region I. Since this region is stable we would expect a stable response. For values of δ_{e0} between -9.5° and -12.2° , the equilibrium value of α is in an unstable region. The trajectory cannot converge to this equilibrium point and it is forced into one of the stable regions that in turn forces it back towards the equilibrium point. Thus we would expect a limit cycle to develop.

This simple analysis allows us to conclude that a limit cycle will develop for certain values of δ_{e0} , and to estimate the onset of the limit cycle as $\delta_{e0} \approx -9.5^\circ$. A more extensive development of this analysis can be found in [35]. In addition, it should be noted that a large amount of qualitative and quantitative work has been done in the general area of piecewise-linear analysis. One advantage of using Volterra submodels will be to reduce the number of regions, which may make analysis more tractable.

Harmonic Balance

To investigate the usefulness of harmonic balance techniques in more complex situations, we consider the following, more accurate, longitudinal model for the aircraft

$$\dot{\alpha} = q + 0.1066 + 0.1097[C_z(\alpha, \delta_e) + C_{zq}(\alpha)q(0.0123)]$$

$$\dot{q} = 5.84[C_m(\alpha, \delta_e) + C_{mq}(\alpha)q(0.0123)]$$

where α is in radians and q in radians/second. Because of its small magnitude, the $C_{zq}(\alpha)$ term will be ignored. The C_z, C_m, C_{mq} functions will be represented by spline fits to wind tunnel data. Plots of these functions are shown in Figures 3-1 (for $\delta_e = -18^\circ$), 4-2, and 4-3.

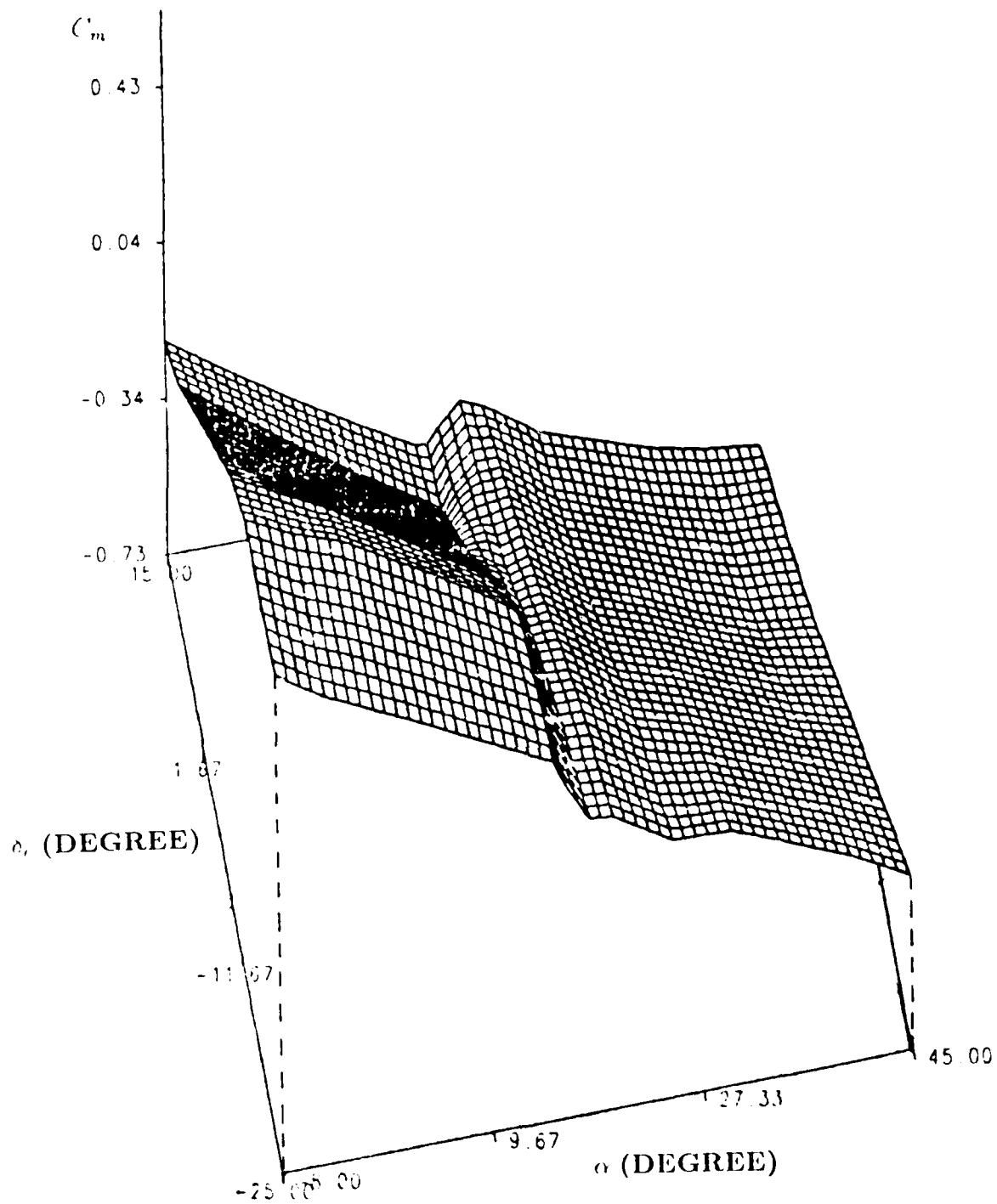


FIGURE 4-2. T-2C WIND TUNNEL DATA: PITCHING MOMENT COEFFICIENT FOR ZERO SIDESLIP.

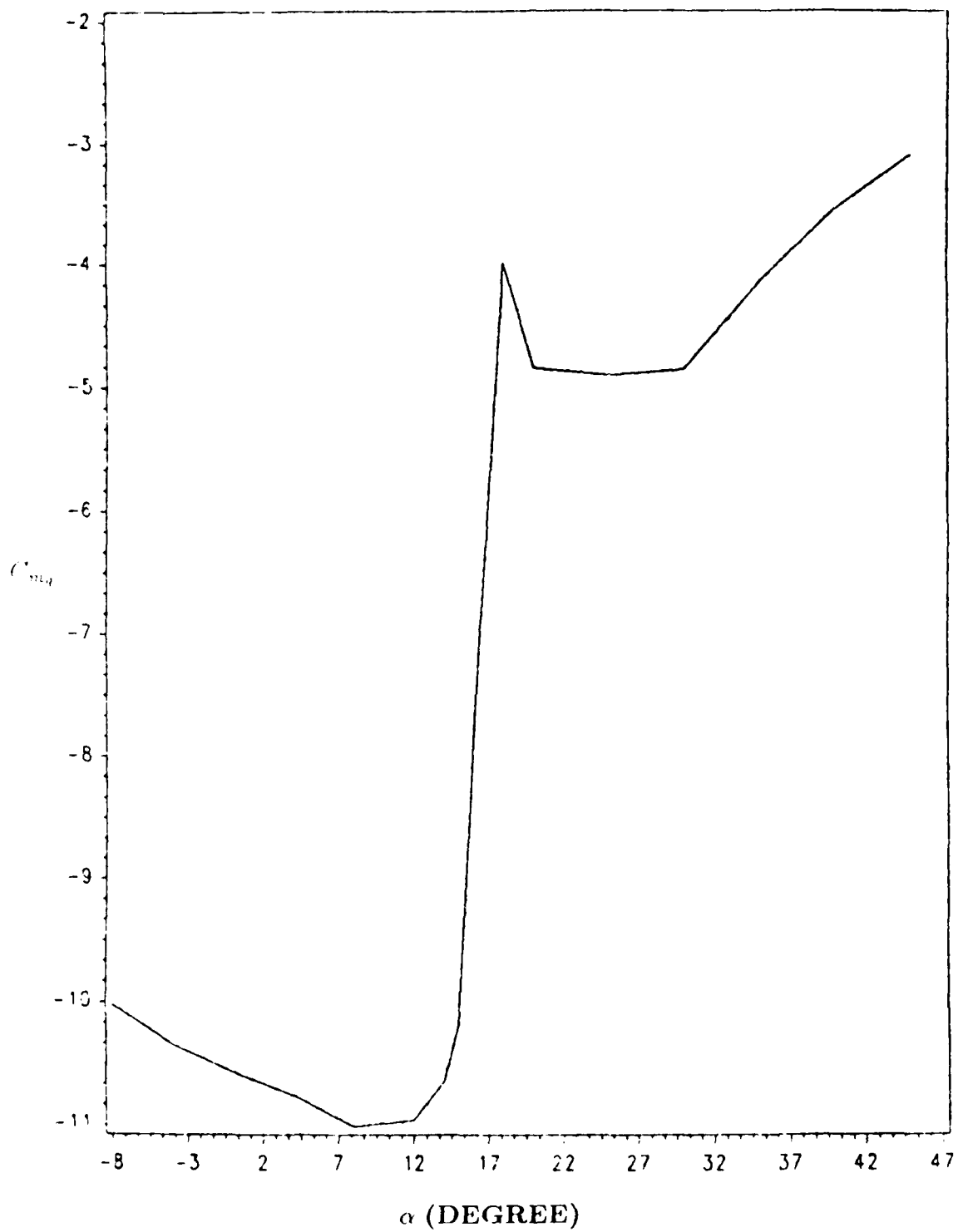


FIGURE 4-3. T-2C C_{m_q} PITCH RATE DERIVATIVE DATA FOR ZERO SIDESLIP.

The most severe nonlinearities occur near $\alpha = 15^\circ$, which is the onset of stall.

Given a constant δ_e , we first assume the solution has the form

$$\alpha(t) = \gamma + a \cos(\omega t)$$

$$q(t) = \gamma_q + a_q \cos(\omega t) + b_q \sin(\omega t).$$

Using a truncated Fourier series, we can approximate the outputs of the nonlinearities by

$$C_m(\alpha(t), \delta_e) = \gamma_m + a_m \cos(\omega t)$$

$$C_z(\alpha(t), \delta_e) = \gamma_z + a_z \cos(\omega t)$$

$$C_{mq}(\alpha(t)) = \gamma_{mq} + a_{mq} \cos(\omega t)$$

where the γ_x and a_x coefficients are computed numerically. Substituting these expressions into the model and retaining only first harmonic terms results in three equations for the unknowns γ , a , and ω . The harmonic balance (numerical) solutions for a and ω are compared with values extracted from time-domain simulation results for three values of δ_e below

δ_e	Harmonic First-Order Balance		Simulation	
	a	ω	a	ω
-15	2.23	4.71	3.15	4.16
-20	3.54	3.56	4.60	3.19
-25	4.35	2.87	5.85	2.73

The values predicted by a first-harmonic analysis are not very accurate.

One problem with the above procedure is that higher harmonic terms in the Fourier expansions of $C_{mq}(\alpha(t))$ and $q(t)$, which were ignored, can "beat down" and affect the constant and first-harmonic terms through the $C_{mq}(\alpha)q$ term in the \dot{q} equation. By considering the multiplicative interaction of the second harmonic of $C_{mq}(\alpha(t))$ with the first harmonic

of q (only one of many higher-order contributions) the improved results given below were obtained.

δ_e	Modified Harmonic First-Order Balance		Simulation	
	a	w	a	w
-15	2.64	4.46	3.15	4.16
-20	4.74	3.21	4.60	3.19
-25	5.87	2.76	5.85	2.73

These results show that with very little additional numerical complexity, it is possible to obtain accurate results outside the stall region. Near stall ($\delta_e \approx -15^\circ$), however, the results degrade.

A more accurate (and complicated) analysis assumes the solution is of the form

$$\alpha(t) = \gamma + a_1 \cos(wt) + a_2 \cos(2wt) + b_2 \sin(2wt) \\ + a_3 \cos(3wt) + b_3 \sin(3wt).$$

Assuming similar Fourier expansions for $q(t)$, $C_m(\alpha(t), \delta_e)$, $C_z(\alpha(t), \delta_e)$ and $C_{mq}(\alpha(t))$, substituting these expressions into the model, and retaining terms through the third harmonic results in seven equations for the unknowns $w, \gamma, a_1, a_2, b_2, a_3, b_3$. Solving these equations produced the following results

δ_e	Harmonic Third-Order Balance		Simulation	
	a	w	a	w
-15	2.96	4.24	3.15	4.16
-20	4.36	3.25	4.60	3.19
-25	5.60	2.75	5.85	2.73

These results show good agreement with simulations even near the onset of stall. From this example, accurate predictions of the amplitude and frequency of the longitudinal limit

cycle near stall, where the nonlinearities are the greatest, require that the effect of higher harmonics be considered. When the nonlinear functions involved in the equations are derived from wind tunnel data, only numerical results will be possible in general.

In summary, the classical methods provide significant insight into the examples considered in this report. For the most part, however, they are limited to assessing stability and predicting limit cycles, and therefore do not form a broad base for the study of nonlinear flying qualities. On the other hand, the Volterra submodels retain the essential characteristics of the nonlinear model, but at this time we do not know how to analytically extract the desired information. The analytical work should be eased somewhat by the fact that the Volterra approach requires fewer regions than the piecewise-linear approach.

5. Conclusion

This work has investigated the use of the Volterra series representation with regard to determining nonlinear flying quality parameters, (also see [5, 36, 37]). Our first goal was to determine if the Volterra series could accurately represent common nonlinear aerodynamic models over the required range of force/moment conditions. We found that by breaking up the state space into natural subspaces in which the nonlinearities could be expressed as low-order polynomials, the total nonlinear model could be represented in each subspace by a low-order, truncated Volterra series. This is a key result, since dealing with the original infinite Volterra series would be intractable. Our simulations showed that the combination of these submodels retained the essential characteristics of the underlying nonlinear model. Since most nonlinearities encountered in practice can be accurately represented locally by polynomials, this technique has general applicability.

Our second goal was to determine if a piecewise-linear model, formed by replacing the nonlinear model by a linear model in each subspace, could accurately capture the nonlinear phenomena contained in the original model. We found that this was not the case. In simulations of a wing rock limit cycle, a piecewise-linear model did not predict the stable limit cycle. Using two-term Volterra models in the same subspaces did predict, via simulations, the existence of a stable limit cycle. In simulations of a longitudinal limit cycle, the piecewise-linear model was significantly less accurate than the low-order Volterra model.

The above results demonstrate that there is a need to go beyond piecewise-linear analysis of nonlinear systems. One appealing feature of the Volterra series is that the "solution" can be written down explicitly, as shown in Section 4.1 for the wing rock example. However, the solution contains so many terms, even for this simple example, that further analysis is necessary in order to extract the important features.

We believe the first priority of future research should be the development of methods for the qualitative and quantitative analysis of multi-region phenomena using Volterra submodels. If such methods can be found the Volterra approach could be a useful tool for nonlinear

flying qualities research.

Our work has also indicated several other areas that would benefit from further research. The first area is the selection of regions and the trim points within regions, and the impact of this selection on the accuracy of the resulting submodels. In the examples considered in this report, the selection was done in an ad hoc manner. The second area is the connection of submodels at the region boundaries. There are several ways in which this can be done and the method used in our examples, initializing the first (linear) Volterra term with the current state and initializing the other terms to zero, may not be optimum.

REFERENCES

1. T.L. Herdman, An application of Volterra series to large amplitude maneuvers, *AFWAL-TM-83-17*, 1983.
2. B. Etkin, *Dynamics of Atmospheric Flight*, John Wiley and Sons, Inc., New York, N.Y., 1972.
3. D. McRuer, Ashkenus, I. and Graham, D., *Aircraft Dynamics and Automatic Control*, Princeton University Press, Princeton, N.J., 1973.
4. A.C. Robinson, On the Quaternions in Simulation of Rigid-Body Motion, *WADC Technical Report 58-17*, Dec. 1958.
5. C.F. Suchomel, Nonlinear flying qualities - one approach, *AIAA-87-0347*, 1987.
6. W.L. Garrard, and J.M. Jordan, Design of Nonlinear Automatic Flight Control Systems, *Automatica*, 13, 497-505. (1977).
7. J.J. Bussgang, L. Ehrman, and J.W. Graham, Analysis of Nonlinear Systems with Multiple Inputs, *Proc IEEE*, Vol. 62, Aug. 1974, 1088-1119.
8. R.W. Brockett, Nonlinear Systems and Differential Geometry, *Proc. IEEE*, Vol. 64, No. 1, 1976, 61-72.
9. R.W. Brockett, Volterra Series and Geometric Control Theory *Automatica*, Vol. 12, 1976, 167-176.
10. R.W. Brockett and E.G. Gilbert, An Addendum to Volterra Series and Geometric Control Theory, *Automatica*, Vol. 12, 1976, 635.
11. P.E. Crouch, Dynamical Realization of Finite Volterra Series, *SIAM J. on Control*, Vol. 19, No. 2, 1981, 177-202.
12. P. D'Alessandro, A. Isidor, and A. Ruberti, Realization and Structure Theory of Bilinear Dynamical Systems, *SIAM J. on Control*, Vol. 12, No. 3, 1974, 517-535.
13. E.G. Gilbert, Functional Expansions for the Response of Nonlinear Differential Systems, *IEEE Transactions on Automatic Control*, Vol. AC-22, Dec. 1977, 909-921.
14. L.R. Hunt, R. Su, and G. Meyer, "Design for Multi-Input Nonlinear Systems," Differential Geometric Control Theory, Birkhauser, New York, NY, *Proc. Conf. MTU*, June 28 - July 2, 1982, pp. 286-298.
15. B.J. Leon and D.J. Schaefer, Volterra Series and Picard Interaction for Nonlinear Circuits and Systems, *IEEE Transactions on Circuits and Systems*, Vol. CAS25, No. 9, Sept. 1978, 789-793.
16. C. Lesiak and A.J. Krener, The Existence and Uniqueness of Volterra Series for Nonlinear Systems, *IEEE Transactions on Automatic Control*, Vol. 23, 1978, 1090-1095.

REFERENCES (Continued)

17. F. Suchomel, An Analytic Solution for a Nonlinear Volterra Technique Capable of Producing Flying Quality Metrics, *AFWAL-TM-87-162FIGC*, 1988.
18. F. Suchomel, A Nonlinear Generic Simulation Model, Preprint.
19. F. Suchomel, An Evaluation of Volterra Series Using a Large Amplitude Aircraft Maneuver, *AFWAL-TM-86-151-FIGC*, Feb. 1986.
20. W.J. Rugh, *Nonlinear System Theory*, The John Hopkins University Press, 1981.
21. M. Schetzen, *The Volterra and Wiener Theories of Nonlinear Systems*, John Wiley and Sons Inc., New York, NY, 1980.
22. H. Stalford, Application of the estimation-before-modeling (EBM) system identification method to the high angle of attack/sideslip flight of the T-2C jet trainer aircraft, Volume III, *Naval Air Development Center Report NADC-76097-30*, April 1979.
23. H.D. Lang and M. Francis, "Unsteady aerodynamics and dynamic aircraft maneuverability," *AGARD Conference Proceedings No. 386*, Unsteady Aerodynamics - Fundamentals and Applications to Aircraft Dynamics, Joint Symposium of the Fluid Dynamics and Flight Mechanics Panels, Gottingen, Federal Republic of Germany, 6-9 May 1985, Paper No. 29.
24. L.T. Nguyen, D. Whipple and J.M. Brandon, "Recent experiences of unsteady aerodynamic effect on aircraft flight dynamics at high angle of attack," *AGARD Conference Proceedings No. 386*, Unsteady Aerodynamics - Fundamentals and Applications to Aircraft Dynamics, joint Symposium of the Fluid Dynamics and Flight Mechanics Panels, Gottingen, Federal Republic of Germany, 6-9 May 1985, Paper No. 28.
25. J.R. Chambers and S.B. Grafton, "Aerodynamic characteristics of airplanes at high angles of attack," *NASA Technical Memorandum 74097*, December 1977.
26. L.T. Nguyen, L. Yip, and J.R. Chambers, Self-induced wing rock of slender delta wings. *AIAA Atmospheric Flight Mechanics Conference*, August 19-21, 1981, Albuquerque, New Mexico.
27. P. Konstadinopoulos, D.T. Mook and A.H. Nayfeh, "Numerical simulation of the subsonic wing-rock phenomenon," *AIAA Atmospheric Flight Mechanics Conference*, AIAA-83-2115, August 15-17, 1983, Gatlinburg, Tennessee.
28. D.G. Murri, L.T. Nguyen and S.B. Grafton, "Wind-tunnel free-flight investigation of a model of a forward-swept-wing flight configuration," *NASA Technical Paper 2230*, February 1984.
29. J.M. Brandon, D.G. Murri and L.T. Nguyen, "Experimental study of effects of forebody geometry on high angle-of-attack static and dynamic stability and control," *15th Congress of the International Council of the Aeronautical Sciences (ICAS)*, September 7-12, 1986, London, England, UK.

REFERENCES (Continued)

30. J.M. Brandon and L.T. Nguyen, Experimental study of effects of forebody geometry on high angle-of-attack static and dynamic stability, *AIAA 24th Aerospace Sciences Meeting*, January 6-9, 1986, Reno, Nevada.
31. Y.W. Jun and R.C. Nelson, "Leading edge vortex dynamics on a delta wing undergoing a wing rock motion," *AIAA 25th Aerospace Sciences Meeting*, January 12-15, 1987, Reno, Nevada, *Paper AIAA-87-0332*.
32. F.H. Lutze, "Curved flow wind tunnel test of a spin-resistant aircraft configuration," *Virginia Polytechnic Institute, Report VPI-Aero-067*, August 1977.
33. F.H. Lutze, "Rolling flow wind tunnel test of a spin resistant aircraft configuration," *Virginia Polytechnic Institute, Report VPI-Aero-075*, December 1977.
34. D.W. Jordan and P. Smith, *Nonlinear Ordinary Differential Equations*, Oxford University Press, 1985.
35. R.E. Kalman, Phase-Plane Analysis of Automatic Control Systems with Nonlinear Gain Elements, *AIEE Transactions*, Vol. 75, pt. II, January, 1955, pp. 383-390.
36. H. L. Stalford, W. T. Baumann, T. L. Herdman and F. E. Garrett, Accurate modelling of nonlinear systems using Volterra series submodels, *1987 American Control Conference*, Minneapolis, MN, June 10-12, 1987, 886-891.
37. W. T. Baumann, T. L. Herdman, H. L. Stalford and C. Suchomel, Recent work using Volterra series as a methodology to analyze nonlinear aircraft dynamics properties, *Proc. of the sixth International Conference on Mathematical Modelling, Mathl Comput. Modelling*, Vol. 11, 883-888.
38. R. K. Miller and A. N. Michel, *Ordinary Differential Equations*, Academic Press, Inc., New York, N. Y., 1982.

LIST OF SYMBOLS

<u>variables</u>	<u>units</u>	<u>Description</u>
α	(deg)	Angle-of-attack
β	(rad)	Angle-of-sideslip
δ_e	(deg)	Elevator control angle
δ_{e_0}	(deg)	Equilibrium elevator control angle
δ_{e_1}	(deg)	Deviation of elevator angle from equilibrium
φ	(rad)	Euler roll angle
A	-	Dynamics of linearized equations (i.e. Jacobian)
b	-	Input matrix for control variable u or δ_e
b	(ft)	Wing span (Section 3.2)
$C_{l\beta}$	(1/rad)	Rolling moment stability derivative due to sideslip β
\tilde{C}_{l_p}	-	Rolling moment derivatives due to roll rate p and sideslip rate $\dot{\beta}$
$C_{m\alpha}$	(1/deg)	Pitching moment derivative w.r.t. α
$C_{m\delta_e}$	(1/deg)	Pitching moment derivative w.r.t. δ_e
C_z	-	Plunging force coefficient (approximates inverted lift coefficient)
g_{i-1}	-	Nonlinear term of i th differential Volterra term
h_i	-	i th order Volterra kernel
k	-	Grouping term parameter in Volterra series expansion
p	(rad/sec)	Roll rate
q	(deg/sec)	Pitch rate
\bar{q}	(lbs/ft ²)	Dynamic pressure
S	(ft ²)	Wing reference area
u	-	Control input

LIST OF SYMBOLS (Continued)

V	(ft/sec)	Free stream speed
x	-	State vector
x^0	-	Initial condition
x_i	-	State vector of i th term in Volterra series expansion
\hat{x}_i	-	State vector of Volterra series approximation with i terms

Appendix A

Volterra Series Representation

In this appendix, we show how the Volterra series arises naturally in the solution of nonlinear ordinary differential equations. The differential form of the series that we have used in this report will be an intermediate step in the calculation of the integral form that has been used by Suchomel [17].

To keep the presentation simple, we consider the scalar, first-order, nonlinear differential equation

$$\dot{x} = x + bx^2 + u. \quad (\text{A.1})$$

The procedure we outline below is general, and can be extended to equations of any order, see Rugh [20].

We consider the solution of (A.1) about the equilibrium point $(x_0, u_0) = (0, 0)$. By considering an input of the form

$$u = ku_1, \quad (\text{A.2})$$

where k is an arbitrary constant, the solution can be written in the form

$$x = kx_1 + k^2x_2 + k^3x_3 + \cdots \quad (\text{A.3})$$

Substituting (A.2) and (A.3) into (A.1), and equating the coefficients of the various powers of k (this calculation has been done in detail for the specific examples considered in the report) yields the set of equations

$$\dot{x}_1 = x_1 + u_1 \quad x_1(0) = 0 \quad (\text{A.4})$$

$$\dot{x}_2 = x_2 + bx_1^2 \quad x_2(0) = 0 \quad (\text{A.5})$$

\vdots

The solution of (A.4) is well known and given by

$$x_1(t) = \int_0^t e^{t-\sigma_1} u_1(\sigma_1) d\sigma_1 \quad (\text{A.6})$$

The first-order Volterra kernel is

$$h_1(t - \sigma_1) = e^{t-\sigma_1}.$$

By considering bx_1^2 to be the input to (A.5), the solution may be written as

$$x_2(t) = \int_0^t e^{t-s} bx_1^2(s) ds.$$

Substituting for $x_1(s)$ from (A.6) gives

$$x_2(t) = \int_0^t e^{(t-s)b} \int_0^s e^{s-\sigma_1} u_1(\sigma_1) d\sigma_1 \int_0^s e^{s-\sigma_2} u_1(\sigma_2) d\sigma_2 ds.$$

To facilitate interchanging the integrals, the upper limits of the nested integrals will be changed from s to t by inserting an appropriate unit-step function

$$\delta_{-1}(z) = \begin{cases} 1 & z \geq 0 \\ 0 & z < 0 \end{cases}.$$

The result is

$$x_2(t) = \int_0^t e^{(t-s)b} \int_0^t \int_0^t \delta_{-1}(s - \sigma_1) e^{s-\sigma_1} u_1(\sigma_1) d\sigma_1 \delta_{-1}(s - \sigma_2) e^{s-\sigma_2} u_1(\sigma_2) d\sigma_2 ds.$$

Changing the order of integration yields

$$x_2(t) = \int_0^t \int_0^t b e^{t-\sigma_1-\sigma_2} \int_0^t e^s \delta_{-1}(s - \sigma_1) \delta_{-1}(s - \sigma_2) ds u_1(\sigma_1) u_1(\sigma_2) d\sigma_1 d\sigma_2$$

The δ_{-1} functions can be eliminated by writing

$$x_2(t) = \int_0^t \int_0^t b e^{t-\sigma_1-\sigma_2} \int_{\max(\sigma_1, \sigma_2)}^t e^s ds u_1(\sigma_1) u_1(\sigma_2) d\sigma_1 d\sigma_2.$$

Evaluating the innermost integral results in

$$x_2(t) = \int_0^t \int_0^t b e^{t-\sigma_1-\sigma_2} [e^t - e^{\max(\sigma_1, \sigma_2)}] u_1(\sigma_1) u_1(\sigma_2) d\sigma_1 d\sigma_2$$

Thus, the second-order Volterra kernel is

$$h_2(t, \sigma_1, \sigma_2) = b e^{t-\sigma_1-\sigma_2} [e^t - e^{\max(\sigma_1, \sigma_2)}]$$

To put this in the time-invariant form $h_2(t - \sigma_1, t - \sigma_2)$ we can write

$$\begin{aligned} h_2(t, \sigma_1, \sigma_2) &= b e^{(t-\sigma_1)} e^{(t-\sigma_2)} e^{-t} [e^t - e^{\max(\sigma_1, \sigma_2)}] \\ &= b e^{(t-\sigma_1)} e^{(t-\sigma_2)} [1 - e^{\max(\sigma_1, \sigma_2)-t}] \\ &= b e^{(t-\sigma_1)} e^{(t-\sigma_2)} [1 - e^{\max(\sigma_1-t, \sigma_2-t)}] \\ &= h_2(t - \sigma_1, t - \sigma_2). \end{aligned}$$

Therefore, the solution can be written in the form

$$\begin{aligned} x(t) &= \int_0^t h_1(t - \sigma_1) u(\sigma_1) d\sigma_1 + \int_0^t \int_0^t h_2(t - \sigma_1, t - \sigma_2) u_1(\sigma_1) u_1(\sigma_2) d\sigma_1 d\sigma_2 \\ &\quad + \dots \end{aligned}$$

which is identical to the form given by (2.1), where the $h_0(t)$ term is equal to zero due to our selection of (0,0) as the equilibrium point.

Appendix B

Longitudinal Equations of Motion

The following longitudinal equations of motion in wind axes for aircraft flight are derived in Etkin [2].

$$\dot{\theta} = q$$

$$\dot{V} = \frac{1}{m}[T_V - D] - g \sin(\theta - \alpha)$$

$$\dot{\alpha} = q + \frac{1}{mV}[T_\alpha - L] + \frac{g}{V} \cos(\theta - \alpha)$$

$$\dot{q} = \left(\frac{qS}{I_y} \right) C_m + \frac{m}{I_y}(l_z X - l_y Z) + \frac{1}{I_y}(l_{z_e} T_x - l_{x_e} T_z)$$

where:

1. The states θ, V, α and q denote pitch angle, air speed, angle-of-attack and pitch rate, respectively.
2. The quantities m and I_y represent the aircraft mass and moment of inertia about the pitch axis y through the center of gravity. The gravity constant is denoted by g .
3. The thrust vector in wind axes is denoted by (T_V, T_α) where T_V is the thrust along the velocity vector. The transformation of thrust from the body axes representation (T_x, T_z) to the wind axes yields the equations

$$T_V = T_x \cos \alpha + T_z \sin \alpha$$

$$T_\alpha = -T_x \sin \alpha + T_z \cos \alpha.$$

4. The aerodynamic forces in wind axes are denoted by drag D and lift L . These are related to the coefficients C_D and C_L of drag and lift, respectively, as follows

$$D = Drag = qSC_D$$

$$L = Lift = \bar{q}SC_L$$

where \bar{q} is dynamic pressure and S is the reference area of the wings.

5. Transforming the drag and lift forces from wind axes to body axes yields the relationships

$$X = -D\cos\alpha + L\sin\alpha$$

$$Z = -D\sin\alpha - L\cos\alpha$$

where X denotes the aerodynamic force along the body x -axis and Z denotes the aerodynamics force along the body z -axis.

6. The aerodynamics pitching moment coefficient is denoted by C_m .

7. The mean aerodynamic chord is represented by \bar{c} .

8. The aerodynamic forces X and Z and the thrust forces T_x and T_z do not necessarily pass through the center of gravity. In general, they have the moment arms l_z, l_y, l_{z_e} and l_{x_e} , respectively, about the center of gravity.

In the above equation, we are assuming that the sideslip angle β is zero. That is, we are considering pure longitudinal motion in the vertical plane - lateral motion is considered to be zero.

In our work we are interested in the cause of the longitudinal limit cycle. We know that it is generated by the nonlinear nature of the lift curve. For this reason we simplify the nonlinear equations. First, we consider only the $\dot{\alpha}$ and the \dot{q} equations. Second, we assume that the moment arms are zero. Third, we use a linear model for the pitching moment as a function of only angle-of-attack α and elevator control δ_e . Fourth, we use a linear model for the elevator control δ_e effect on lift. According to the assumptions we can write

$$C_L = C_L(\alpha) + C_{L_{\delta_e}} \delta_e$$

$$C_m = C_{m_0} + C_{m_\alpha} \alpha + C_{m_{\delta_e}} \delta_e$$

Since $C_L(\alpha) = -\frac{C_z(\alpha)}{\cos(\alpha)} - C_D(\alpha)\tan(\alpha)$

we have the approximation

$$C_L(\alpha) \cong -C_z(\alpha) + c_7, \quad 10^\circ \leq \alpha \leq 20^\circ$$

where c_7 is some constant. We make the definitions

$$c_1 = \frac{\bar{q}S}{mV}$$

$$c_2 = -\frac{\bar{q}S}{mV} C_{L_{\delta_e}}$$

$$c_3 = \frac{T_\alpha}{mV} + \frac{g}{V} \cos(\theta - \alpha) - \frac{\bar{q}S}{mV} c_7$$

$$c_4 = \frac{\bar{q}S\bar{c}}{I_y} C_{m_\alpha}$$

$$c_5 = \frac{\bar{q}S\bar{c}}{I_y} C_{m_{\delta_e}}$$

$$c_6 = \frac{\bar{q}S\bar{c}}{I_y} C_{m_0}$$

The resulting equations simplify to the following:

$$\dot{\alpha} = q + c_1 C_z(\alpha) + c_2 \delta_e + c_3$$

$$\dot{q} = c_4 \alpha + c_5 \delta_e + c_6$$

where $c_i, i = 1, 2, \dots, 6$ are treated as constants, and where $C_z(\alpha)$ is to be chosen from the real data of some airplane. For the T-2C airplane of Ref. 22, the following approximate model is obtained.

$$\dot{\alpha} = q + 9.17C_z(\alpha) - 1.8(\delta_e + 7^\circ) + 7.36$$

$$\dot{q} = 5.73(C_{m_\alpha}\alpha + C_{m_{\delta_e}}\delta_e) + 2.9$$

where $C_{m_\alpha} = -1$, $C_{m_{\delta_e}} = -1.5$ and where the nonlinearities of the $C_z(\alpha)$ curve can be represented by the following low-order subspace models:

$$\alpha \leq 14.4^\circ, \quad C_z(\alpha) \cong -0.0732\alpha$$

$$14.4^\circ \leq \alpha \leq 15.6^\circ, \quad C_z(\alpha) \cong 0.1\alpha^2 - 2.9\alpha + 20.0$$

$$15.6^\circ \leq \alpha \leq 19.6^\circ, \quad C_z(\alpha) \cong -0.02\alpha^2 + 0.74\alpha - 7.8$$

$$19.6^\circ \leq \alpha \leq 28^\circ, \quad C_z(\alpha) \cong -0.47 - 0.02\alpha.$$

These subspace models are curve-fits to the actual post flight aerodynamic data of the T-2C obtained by system identification analysis, [22]. We note that these aerodynamic derivatives represent approximate values for the total airplane. The above model may lack continuity at the boundary points since all numbers have been rounded off. The model given in Section 3 has less round-off error associated with it, and as a consequence there is continuity at the boundaries. This continuity is with respect to the curve but not necessarily with respect to the slope.

Appendix C

Volterra Expansion for Longitudinal Example

In this appendix we present the details of the Volterra expansion for region II ($14.36^\circ \leq \alpha \leq 15.6^\circ$) of the longitudinal limit cycle example considered in Section 3.1. The expansion for region III is similar, and the equation is linear in the other regions.

The simplified longitudinal equations are

$$\dot{\alpha} = q + 9.168 C_z(\alpha) - 1.8336(\delta_e + 7^\circ) + 7.3619 \quad (\text{C.1})$$

$$\dot{q} = 5.73(-\alpha - 1.5\delta_e) + 2.865. \quad (\text{C.2})$$

In region II we have

$$C_z(\alpha) = 0.09722\alpha^2 - 2.8653\alpha + 20.03846. \quad (\text{C.3})$$

Substituting (C.3) into (C.1), (C.2) and rearranging gives

$$\dot{x} = \begin{bmatrix} q + 0.8913\alpha^2 - 26.269\alpha + 178.24 \\ -5.73\alpha + 2.865 \end{bmatrix} + \begin{bmatrix} -1.8336 \\ -8.595 \end{bmatrix} \delta_e \quad (\text{C.4})$$

where $x = \begin{bmatrix} \alpha \\ q \end{bmatrix}$.

Considering an input of the form

$$\delta_e = \delta_{e0} + k\delta_{e1} \quad (\text{C.5})$$

the solution of (C.4) may be written in the form

$$x = x_0 + kx_1 + k^2x_2 + k^3x_3 + \dots \quad (\text{C.6})$$

The equilibrium input in region II was chosen to be $\delta_{e0} = -9.24^\circ$. This resulted in the equilibrium state $x_0 = [14.36^\circ, -1.7552^\circ/\text{sec}]^T$. Substituting (C.5), (C.6) into (C.4) results in

$$k\dot{x}_1 + k^2\dot{x}_2 + k^3\dot{x}_3 + \dots =$$

$$\left[\begin{array}{c} (q_0 + kq_1 + \dots) + .8913(\alpha_0 + k\alpha_1 + \dots)^2 - 26.269(\alpha_0 + k\alpha_1 + \dots) + 178.24 \\ -5.73(\alpha_0 + k\alpha_1 + \dots) + 2.865 \end{array} \right]$$

$$+ \left[\begin{array}{c} -1.8336 \\ -8.595 \end{array} \right] (\delta_{e_0} + k\delta_{e_1}).$$

Using the equilibrium values, expanding terms, and keeping terms up to order 3 in k yields

$$k\dot{x}_1 + k^2\dot{x}_2 + k^3\dot{x}_3 =$$

$$\left[\begin{array}{c} k(-0.6709\alpha_1 + q_1 - 1.8336\delta_{e_1}) + k^2(-0.6709\alpha_2 + 0.8913\alpha_1^2 + q_2) \\ k(-5.73\alpha_1 - 8.595\delta_{e_1}) + k^2(-5.73\alpha_2) \end{array} \right]$$

$$+ \left[\begin{array}{c} k^3(-0.6709\alpha_3 + 1.7826\alpha_1\alpha_2 + q_3) \\ k^3(-5.73\alpha_3) \end{array} \right].$$

Equating coefficients of equal powers of k yields the following equations for the Volterra series terms.

$$\dot{x}_1 = \begin{bmatrix} -0.6709 & 1 \\ -5.73 & 0 \end{bmatrix} x_1 + \begin{bmatrix} -1.8336 \\ -8.595 \end{bmatrix} \delta_{e_1}$$

$$\dot{x}_2 = \begin{bmatrix} -0.6709 & 1 \\ -5.73 & 0 \end{bmatrix} x_2 + \begin{bmatrix} 0.8913\alpha_1^2 \\ 0 \end{bmatrix}$$

$$\dot{x}_3 = \begin{bmatrix} -0.6709 & 1 \\ -5.73 & 0 \end{bmatrix} x_3 + \begin{bmatrix} 1.7826\alpha_1\alpha_2 \\ 0 \end{bmatrix}.$$

Appendix D

Wing Rock Model

Aircraft configurations incorporating slender forebodies generate a wing rock limit cycle phenomenon at high α (angle-of-attack) due to unsteady aerodynamic effects, [23 - 33]. Delta wings with leading edge sweeps greater than 76° are known to exhibit wing rock. Nguyen, Whipple and Brandon [24] present wind-tunnel testing results of such an 80° delta wing. The F-5 airplane which has a slender forebody is known to exhibit wing rock at high α . Lutze [32,33] presents wind-tunnel lateral-directional aerodynamics data of a 10-percent-scale model of the F-5E airplane. A wind-tunnel investigation of a 16-percent-scale model of the X-29A airplane (which has the same nose section as the F-5 airplane) is described in Murri, Nguyen and Grafton [28]. Using the data contained in these references we construct a wing rock model. First, we investigate the aerodynamic properties of the 80° delta wing that is inherent in wing rock. We inspected the scaled X-29A wind-tunnel model and found it to exhibit similar wing rock model characteristics as the 80° delta wing. For this reason we construct our model based on the 80° delta wing data, [24].

The standard wind-tunnel test technique used in the study of wing rock phenomenon is the free-to-roll tests. In these tests the physical scaled model is sting mounted on an apparatus which allows the model to rotate freely about its roll axis (i.e., the body x -axis) with no angular limitation. A 80° delta wing mounted on such an apparatus is shown in Figure 2 of Nguyen, Whipple and Brandon [24]. The resulting system is a single degree of freedom (SDOF) system. To keep our presentation as simple as possible without loss of qualitative significance, we consider a mathematical model of wing rock resulting from such a wind-tunnel testing apparatus.

In a free-to-roll test, the pitch angle θ , which is fixed, is preset according to the desired angle-of-attack (α) at zero sideslip ($\beta = 0^\circ$). The roll angle φ denotes the angle of roll about

the longitudinal body x -axis.

Let V be the total airspeed. The conventional definitions of the body axes velocity components (u, v, w) are

$$u = V \cos(\theta)$$

$$v = V \sin(\theta) \sin(\phi)$$

$$w = V \sin(\theta) \cos(\phi)$$

and the angle-of-attack and the sideslip angle satisfy the identities

$$\tan(\alpha) = \frac{w}{u}$$

$$\sin(\beta) = \frac{v}{V}.$$

From these we have the identities

$$\tan(\beta) = \frac{v}{\sqrt{u^2 + w^2}}$$

$$\sin(\alpha) = \frac{w}{\sqrt{u^2 + w^2}}$$

$$\tan(\varphi) = \frac{v}{w}$$

$$\cos(\theta) = \frac{u}{v}$$

$$\cos(\alpha) = \frac{u}{\sqrt{u^2 + w^2}}$$

$$\cos(\beta) = \frac{\sqrt{u^2 + w^2}}{V}$$

$$\sin(\theta) = \frac{\sqrt{v^2 + w^2}}{V}$$

$$\cos(\varphi) = \frac{w}{\sqrt{v^2 + w^2}}$$

$$\sin(\varphi) = \frac{v}{\sqrt{v^2 + w^2}}.$$

Observe that

$$\dot{\beta} = \frac{\dot{v}}{V \cos(\beta)}$$

$$\dot{\varphi} = \frac{\dot{v}}{\cos(\varphi)\sqrt{V^2 - u^2}}.$$

Since u and V are constant functions of time. From these it follows that

$$\dot{\beta} = \dot{\varphi} \frac{\cos(\varphi)\sqrt{v^2 + w^2}}{\cos(\beta)V}$$

or, equivalently,

$$\dot{\beta} = \dot{\varphi} \frac{\cos(\varphi)}{\cos(\beta)} \sin(\theta).$$

The angle of attack α and sideslip angle β are functions of θ and φ and satisfy the following relationships,

$$\tan(\alpha) = \tan(\theta)\cos(\varphi) \quad (\text{D.1})$$

$$\sin(\beta) = \sin(\theta)\sin(\varphi) \quad (\text{D.2})$$

$$\tan(\beta) = \sin(\alpha)\tan(\varphi) \quad (\text{D.3})$$

$$\cos(\theta) = \cos(\alpha)\cos(\beta) \quad (\text{D.4})$$

$$\sin(\alpha) = \frac{\sin(\theta)\cos(\varphi)}{\cos(\beta)} \quad (\text{D.5})$$

$$\dot{\beta} = \dot{\varphi}\sin(\alpha). \quad (\text{D.6})$$

In our construction of a wing rock model it suffices to consider the following approximation to Equation (D.3), using small angles in β and φ :

$$\beta = \varphi\sin(\alpha). \quad (\text{D.7})$$

The roll rate p satisfies

$$\dot{\varphi} = p. \quad (\text{D.8})$$

The motion about the roll axis is governed by the nondimensional aerodynamic rolling moment coefficient C_l which is a function of $\alpha, \beta, p, \dot{\beta}$ and δ_a :

$$\dot{p} = \left(\frac{\bar{q}Sb}{I_x} \right) C_l(\alpha, \beta, p, \dot{\beta}, \delta_a) \quad (\text{D.9})$$

where

$\bar{q} = \frac{1}{2}\rho(h)V^2 = \text{free stream dynamic pressure}$

$\rho(h)$ - standard air density at altitude h

S = wing reference area

b = wing span

I_x = roll moment of inertia

δ_a = aileron control surface deflection angle.

The rolling moment coefficient C_l has the expansion

$$C_l(\alpha, \beta, p, \dot{\beta}, \delta_a) = C_{l_\beta}(\alpha)\beta + \bar{C}_{l_p}(\alpha, \beta)\frac{pb}{2V} + C_{l_{\delta_a}}(\alpha, \beta)\delta_a \quad (\text{D.10})$$

where

$$\bar{C}_{l_p}(\alpha, \beta) = C_{l_p}(\alpha, \beta) + C_{l_\beta}(\alpha, \beta)\sin(\alpha) \quad (\text{D.11a})$$

and where, from (D.6) and (D.8),

$$C_{l_\beta}(\alpha, \beta)\frac{\dot{\beta}b}{2V} = C_{l_\beta}(\alpha, \beta)\sin(\alpha)\frac{pb}{2V} \quad (\text{D.11b})$$

Using (D.7) and (D.10) we rewrite (D.9) in the standard form

$$\dot{p} + \omega_n^2(\alpha)\varphi + 2\omega_n(\alpha)\zeta(\alpha, \varphi)p = f(\alpha, \beta)\delta_a \quad (\text{D.12})$$

where

$$\omega_n^2(\alpha) = -\left(\frac{\bar{q}Sb}{I_x}\right)C_{l_\beta}(\alpha)\sin(\alpha) \quad (\text{D.13})$$

$$2\omega_n(\alpha)\zeta(\alpha, \varphi) = -\left(\frac{\bar{q}Sb}{I_x}\right)\left(\frac{b}{2V}\right)\bar{C}_{l_p}(\alpha, \beta = \varphi\sin\alpha) \quad (\text{D.14})$$

$$f(\alpha, \beta) = \left(\frac{\bar{q}Sb}{I_x}\right)C_{l_{\delta_a}}(\alpha, \beta). \quad (\text{D.15})$$

In order for the system (D.8) and (D.12) to be stable at high α it is necessary that the signs of $C_{\ell_\beta}(\alpha)$ and $\bar{C}_{\ell_p}(\alpha, \beta)$ both be negative. The sign of $C_{\ell_\beta}(\alpha)$ is indeed negative at high α . We remark that $\bar{C}_{\ell_p}(\alpha, \beta)$ has a negative sign at low α . But airplanes that exhibit wing rock at high α , $25^\circ \leq \alpha \leq 50^\circ$, have a coefficient derivative $\bar{C}_{\ell_p}(\alpha, \beta)$ that is positive for small sideslip angles and negative for large sideslip angles, Nguyen, Whipple and Brandon [24] and Murri, Nguyen and Grafton [28]. The wing rock limit cycle phenomenon results from this switch in sign of $\bar{C}_{\ell_p}(\alpha, \beta)$ from positive to negative at high α as the sideslip angle increases to large amplitudes.

In order to make use of Eq. (D.10) we need (quantitative) expressions for the aerodynamic derivatives $C_{\ell_\beta}(\alpha)$ and $\bar{C}_{\ell_p}(\alpha, \beta)$. Wind Tunnel model data provides $C_{\ell_\beta}(\alpha)$ and $\bar{C}_{\ell_p}(\alpha, \beta)$ in graphic form. We remark that wind tunnel model data provides a model for the left-hand side of Eq. (D.11a) but it does not provide separate models of the terms $C'_{\ell_p}(\alpha, \beta)$ and $C'_{\ell_\beta}(\alpha, \beta)$ on the right-hand side. The model given below in Eqs. (D.16) and (D.17) is an approximation to the wind tunnel data plots contained in [24].

The model of $\bar{C}_{\ell_p}(\alpha, \beta)$ presented in Nguyen, Whipple and Brandon, [24], for the 80° delta wing is typical of airplanes exhibiting wing rock at high α . Their model can be approximated by the following:

NASA WIND-TUNNEL STING MOUNTED MODEL 80° delta wing

$$C'_{\ell_p}(\alpha = 30^\circ, \beta) = 0.4[1 - 7.64|\beta|], \quad 0 \leq |\beta| \leq 0.35 \quad (D.16)$$

$$C'_{\ell_\beta}(\alpha = 30^\circ) = -0.4584 \quad (D.17)$$

$$\varphi = 2\beta \quad (\beta = \varphi \sin \alpha \text{ at } \alpha = 30^\circ) \quad (D.18)$$

$$\frac{1}{2} \left(\frac{qSb}{I_x} \right) C'_{\ell_\beta}(\alpha = 30^\circ) = -26.6667 \quad (D.19)$$

$$\left(\frac{qSb}{I_x} \right) \left(\frac{b}{2I_y} \right) C'_{\ell_p}(\alpha = 30^\circ, \varphi) = .76485[1 - 3.821|\varphi|] \quad (D.20)$$

so that

$$\dot{p} = -26.6667\varphi + 0.76485[1 - 3.82|\varphi|]p \quad (\text{D.21})$$

There are no control surfaces on their wind-tunnel model. Therefore, the $f(\alpha, \beta)$ term drops out. The above model is used in the Volterra Series analysis of Section 3.2.

Appendix E

Expansion of Volterra Series for Wing Rock Example

The model for wing rock as derived in Appendix D is given by

$$\dot{\varphi} = p$$

$$\dot{p} = -26.7\varphi + 0.76[1 - 3.82|\varphi|]p.$$

We can represent this equation with respect to the following two regions:

Region I: $\varphi > 0$

$$\dot{p} = -26.7\varphi + 0.76[1 - 3.82\varphi]p$$

Region II: $\varphi < 0$

$$\dot{p} = -26.7\varphi + 0.76[1 + 3.82\varphi]p.$$

We note that the \dot{p} equation is bilinear in the φp term.

A state space representation of the nonlinear equation is given by

$$\begin{bmatrix} \dot{\varphi} \\ \dot{p} \end{bmatrix} = \begin{bmatrix} 0 & 1 \\ -26.7 & 0.76 \end{bmatrix} \begin{bmatrix} \varphi \\ p \end{bmatrix} + \begin{bmatrix} 0 \\ (-1)^i 2.92\varphi p \end{bmatrix}, \quad i = 1, 2.$$

Let $x = \begin{bmatrix} \varphi \\ p \end{bmatrix}$ and express the system as

$$\dot{x} = Ax + \begin{bmatrix} 0 \\ (c)NL \text{ term} \end{bmatrix}, \quad c = (-1)^i 2.92, \quad i = 1, 2.$$

Using the Volterra Series technique described in Section 2, we represent the nonlinear solutions $\varphi(t)$ and $p(t)$ as the infinite expressions

$$\varphi(t) = \varphi_0 + \varphi_1(t)k + \varphi_2(t)k^2 + \cdots + \varphi_n(t)k^n + \cdots$$

$$p(t) = p_0 + p_1(t)k + p_2(t)k^2 + \dots + p_n(t)k^n + \dots$$

$$(\varphi_0, p_0) = (0, 0) \text{ equilibrium point (unstable).}$$

Taking the product of $\varphi(t)$ and $p(t)$, collecting terms with respect to like powers of k and taking into account the equilibrium point yield

$$\varphi p = (\varphi_1 p_1)k^2 + (\varphi_1 p_2 + \varphi_2 p_1)k^3 + (\varphi_1 p_3 + \varphi_2 p_2 + \varphi_3 p_1)k^4 + \dots$$

We make the identifications:

$$g_{12}(x_1) = \varphi_1 p_1$$

$$g_{22}(x_1, x_2) = \varphi_1 p_2 + \varphi_2 p_1$$

$$g_{33}(x_1, x_2, x_3) = \varphi_1 p_3 + \varphi_2 p_2 + \varphi_3 p_1$$

$$\varphi p = g_{12}(x_1)k^2 + g_{22}(x_1, x_2)k^3 + g_{32}(x_1, x_2, x_3)k^4 + \dots$$

The Volterra Series approximation of the nonlinear equation is therefore given by:

$$\dot{x}_1 = Ax_1$$

$$\dot{x}_2 = Ax_2 + g_1(x_1), \quad g_1(x_1) = \begin{bmatrix} 0 \\ cg_{12}(x_1) \end{bmatrix}, \quad c = (-1)^j 2.92, \quad j = 1, 2$$

$$\dot{x}_3 = Ax_3 + g_2(x_1, x_2), \quad g_2(x_1, x_2) = \begin{bmatrix} 0 \\ cg_{22}(x_1, x_2) \end{bmatrix}$$

$$\dot{x}_n = Ax_n + g_{n-1}(x_1, \dots, x_{n-1}), \quad g_{n-1}(x_1, \dots, x_{n-1}) = \begin{bmatrix} 0 \\ cg_{(n-1)2}(x_1, \dots, x_{n-1}) \end{bmatrix}$$

$$\text{where } x_i = \begin{bmatrix} \varphi_i \\ p_i \end{bmatrix} \quad i = 1, \dots, n, \dots$$

Appendix F

Two-Term Volterra Series Approximation

In this appendix we present the details of the Volterra series analysis for the wing rock example discussed in Section 4.1. As requested by the contract monitor, all derivations needed to obtain the two-term Volterra series approximation $\hat{x}_2(t) = x_1(t) + x_2(t)$ for the system (4.1), thus (4.2), are presented here for the region $\varphi \geq 0$. The 2×2 matrix A and the constants a, b, c as well as the 2×1 vector functions x, g are as defined in Section 4.1. From (4.5) and (4.6) we see that the 2×1 vector functions $x_1(t)$ and $x_2(t)$ satisfy

$$\dot{x}_1 = Ax_1(t), \quad x_1(0) = x^0 = \begin{bmatrix} 0 \\ p^0 \end{bmatrix} \quad (\text{F.1})$$

$$\dot{x}_2(t) = Ax_2(t) + \begin{bmatrix} 0 \\ -cx_{11}(t)x_{12}(t) \end{bmatrix}, \quad x_2(0) = 0 \quad (\text{F.2})$$

where

$$x_1(t) = \begin{bmatrix} x_{11}(t) \\ x_{12}(t) \end{bmatrix}, \quad x_2(t) = \begin{bmatrix} x_{21}(t) \\ x_{22}(t) \end{bmatrix}.$$

Solving for $x_1(t)$ in (F.1)

Equation (F.1) is a first-order linear ordinary differential equation with constant coefficient matrix A . Eigenvalues for the matrix A are $\lambda_1 = (b + \sqrt{b^2 - 4a})/2$ and $\lambda_2 = (b - \sqrt{b^2 - 4a})/2$. Note that $b^2 - 4a < 0$ thus $\lambda_1 = (b/2) + i\omega_0$ and $\lambda_2 = (b/2) - i\omega_0$ where $\omega_0 \equiv (\sqrt{4a - b^2})/2$. The matrix exponential e^{At} , the state transition matrix for (F.1), can be computed by the identity (see Miller [38, page 111])

$$e^{At} = w_1(t)I + w_2(t)(A - \lambda_1 I) \quad (\text{F.3})$$

where I is the 2×2 identity matrix and the scalar functions w_1 and w_2 satisfy

$$\dot{w}_1(t) = \lambda_1 w_1(t), \quad w_1(0) = 1 \quad (\text{F.4})$$

and

$$\dot{w}_2(t) = \lambda_2 w_2(t) + w_1(t), \quad w_2(0) = 0. \quad (\text{F.5})$$

It now follows that

$$w_1(t) = e^{\lambda_1 t} \quad (\text{F.6})$$

and

$$\begin{aligned} w_2(t) &= e^{\lambda_2 t} \int_0^t e^{-\lambda_2 s} w_2(s) ds \\ &= e^{\lambda_2 t} \int_0^t e^{s(\lambda_1 - \lambda_2)} ds \\ &= \frac{e^{\lambda_2 t}}{\lambda_1 - \lambda_2} [e^{t(\lambda_1 - \lambda_2)} - 1], \quad (\lambda_1 - \lambda_2) \neq 0 \\ &= \frac{e^{\lambda_1 t} - e^{\lambda_2 t}}{\lambda_1 - \lambda_2}. \end{aligned} \quad (\text{F.7})$$

Using identities (F.6) and (F.7) in (F.3) yield

$$\begin{aligned} e^{At} &= e^{\lambda_1 t} I + \frac{e^{\lambda_1 t} - e^{\lambda_2 t}}{\lambda_1 - \lambda_2} (A - \lambda_1 I) \\ &= e^{bt/2} \left[e^{i\omega_0 t} I + \frac{e^{i\omega_0 t} - e^{-i\omega_0 t}}{\lambda_1 - \lambda_2} (A - \lambda_1 I) \right] \\ &= e^{bt/2} \left[e^{i\omega_0 t} I + \frac{2i \sin \omega_0 t}{2i\omega_0} (A - \lambda_1 I) \right] \\ &= e^{bt/2} \left\{ e^{i\omega_0 t} I + \frac{\sin \omega_0 t}{\omega_0} \begin{bmatrix} -\lambda_1 & 1 \\ -a & b - \lambda_1 \end{bmatrix} \right\} \\ &= e^{bt/2} \left[\begin{array}{cc} e^{i\omega_0 t} - \frac{\lambda_1 \sin \omega_0 t}{\omega_0} & \frac{\sin \omega_0 t}{\omega_0} \\ -\frac{a \sin \omega_0 t}{\omega_0} & e^{i\omega_0 t} + \frac{(b - \lambda_1) \sin \omega_0 t}{\omega_0} \end{array} \right] \end{aligned}$$

which gives the identity

$$e^{At} = e^{bt/2} \begin{bmatrix} \cos\omega_0 t - \frac{b \sin\omega_0 t}{2\omega_0} & \frac{\sin\omega_0 t}{\omega_0} \\ -\frac{a \sin\omega_0 t}{\omega_0} & \cos\omega_0 t + \frac{b \sin\omega_0 t}{2\omega_0} \end{bmatrix}.$$

Let $B_{ij}(t)$ denote the i^{th} row- j^{th} column entry in the above matrix, see equation (4.7). The solution $x_1(t)$ for the initial value problem (F.1) is given by

$$x_1(t) = e^{At} \begin{bmatrix} 0 \\ p^0 \end{bmatrix} = e^{bt/2} p^0 \begin{bmatrix} B_{12}(t) \\ B_{22}(t) \end{bmatrix}. \quad (\text{F.8})$$

Solving for $x_2(t)$ in (F.2)

Equation (F.2) is a first-order linear ordinary differential equation with a nonzero forcing function

$$\begin{bmatrix} 0 \\ -cx_{11}(t)x_{12}(t) \end{bmatrix}$$

where from above $x_{11}(t) = e^{bt/2} p^0 B_{12}(t)$ and $x_{12}(t) = e^{bt/2} p^0 B_{22}(t)$. The variation of constants formula together with the zero initial conditions of (F.2) yields

$$x_2(t) = (p^0)^2 \int_0^t e^{A(t-\tau)} \begin{bmatrix} 0 \\ -c \end{bmatrix} e^{b\tau} B_{12}(\tau) B_{22}(\tau) d\tau.$$

We now employ the above calculation of e^{At} (in terms of the $B_{ij}(t)$ functions defined above) to express $x_2(t)$ by

$$x_2(t) = (p^0)^2 e^{At} \int_0^t e^{-A\tau} \begin{bmatrix} 0 \\ 1 \end{bmatrix} (-c) e^{b\tau} B_{12}(\tau) B_{22}(\tau) d\tau$$

$$x_2(t) = -c(p^0)^2 e^{At} \int_0^t e^{-b\tau/2} \begin{bmatrix} B_{12}(-\tau) \\ B_{22}(-\tau) \end{bmatrix} e^{b\tau} B_{12}(\tau) B_{22}(\tau) d\tau$$

$$x_2(t) = -c(p^0)^2 e^{At} \int_0^t e^{b\tau/2} \begin{bmatrix} B_{12}(-\tau) \\ B_{22}(-\tau) \end{bmatrix} B_{12}(\tau) B_{22}(\tau) d\tau. \quad (\text{F.9})$$

The matrix e^{At} is nonsingular and has an inverse e^{-At} . We shall now note that $p^0 \neq 0$ and use (F.9) to obtain

$$-\frac{e^{-At}x_2(t)}{c}(p^0)^{-2} = \int_0^t e^{b\tau/2} \begin{bmatrix} B_{12}(-\tau) \\ B_{22}(-\tau) \end{bmatrix} B_{12}(\tau) B_{22}(\tau) d\tau. \quad (\text{F.10})$$

We now direct our attention to the first row of the right hand side of (F.10).

$$\begin{aligned} R_{11}(t) &\equiv \int_0^t e^{b\tau/2} B_{12}(-\tau) B_{12}(\tau) B_{22}(\tau) d\tau \\ &= -\frac{1}{\omega_0^2} \int_0^t e^{b\tau/2} \sin^2 \omega_0 \tau \cos \omega_0 \tau d\tau - \frac{b}{2\omega_0^3} \int_0^t e^{b\tau/2} \sin^3 \omega_0 \tau d\tau \end{aligned}$$

$$\left(\begin{array}{l} \text{Integration by parts: } u = e^{b\tau/2}, dv = \sin^2 \omega_0 \tau \cos \omega_0 \tau d\tau \\ du = \frac{b}{2} e^{b\tau/2} d\tau, v = \frac{\sin^3 \omega_0 \tau}{3\omega_0} \end{array} \right)$$

$$R_{11}(t) = -\frac{1}{\omega_0^2} \left\{ e^{b\tau/2} \frac{\sin^3 \omega_0 \tau}{3\omega_0} \Big|_{\tau=0}^{\tau=t} - \int_0^t \frac{b}{6\omega_0} e^{b\tau/2} \sin^3 \omega_0 \tau d\tau \right\}$$

$$- \frac{b}{2\omega_0^3} \int_0^t e^{b\tau/2} \sin^3 \omega_0 \tau d\tau$$

$$R_{11}(t) = -\frac{e^{bt/2} \sin^3 \omega_0 t}{3\omega_0^3} - \frac{b}{3\omega_0^3} \int_0^t e^{b\tau/2} \sin^3 \omega_0 \tau d\tau.$$

For the second row of the function on the right-hand side of (F.10) we have

$$R_{21}(t) = \int_0^t e^{b\tau/2} B_{22}(-\tau) B_{22}(\tau) B_{12}(\tau) d\tau$$

$$R_{21}(t) = \int_0^t e^{b\tau/2} (\cos^2 \omega_0 \tau - \frac{b^2}{4\omega_0^2} \sin^2 \omega_0 \tau) \frac{\sin \omega_0 \tau}{\omega_0} d\tau$$

$$R_{21}(t) = \int_0^t \frac{e^{b\tau/2}}{\omega_0} [1 - (1 + \frac{b^2}{4\omega_0^2}) \sin^2 \omega_0 \tau] \sin \omega_0 \tau d\tau$$

$$R_{21}(t) = \int_0^t \frac{e^{b\tau/2}}{\omega_0} \sin \omega_0 \tau d\tau - \int_0^t \frac{e^{b\tau/2}}{\omega_0} (1 + \frac{b^2}{4\omega_0^2}) \sin^3 \omega_0 \tau d\tau$$

We now integrate the first term on the right to obtain

$$R_{21}(t) = \frac{4}{\omega_0(b^2 + 4\omega_0^2)} [e^{bt/2} (\frac{b}{2} \sin \omega_0 t - \omega_0 \cos \omega_0 t) + \omega_0] \\ - \int_0^t \frac{e^{b\tau/2}}{\omega_0} (1 + \frac{b^2}{4\omega_0^2}) \sin^3 \omega_0 \tau d\tau.$$

In order to eliminate the integral terms from both $R_{11}(t)$ and $R_{21}(t)$ we note that (see integration tables)

$$\int_0^t e^{b\tau/2} \sin^3 \omega_0 \tau d\tau = \frac{4}{b^2 + 36\omega_0^2} \{ (\frac{b}{2} \sin \omega_0 t + -3\omega_0 \cos \omega_0 t) e^{bt/2} \sin^2 \omega_0 t \\ + 6\omega_0^2 \int_0^t e^{b\tau/2} \sin \omega_0 \tau d\tau \}.$$

Integrating the last term gives

$$\int_0^t e^{b\tau/2} \sin^3 \omega_0 \tau d\tau = \frac{4}{b^2 + 36\omega_0^2} \{ (\frac{b}{2} \sin \omega_0 t - 3\omega_0 \cos \omega_0 t) e^{bt/2} \sin^2 \omega_0 t \\ + \frac{24\omega_0^2}{b^2 + 4\omega_0^2} e^{bt/2} (-\omega_0 \cos \omega_0 t + \frac{b}{2} \sin \omega_0 t) \\ + \frac{24\omega_0^3}{b^2 + 4\omega_0^2} \}$$

$$(\text{Note: } b^2 + 4\omega_0^2 = b^2 + 4 \frac{(4a - b^2)}{4} = 4a)$$

$$\begin{aligned} &= \frac{2b}{b^2 + 36\omega_0^2} e^{bt/2} \sin^3 \omega_0 t - \frac{12\omega_0}{b^2 + 36\omega_0^2} e^{bt/2} \sin^2 \omega_0 t \cos \omega_0 t \\ &\quad - \frac{24\omega_0^3}{a(b^2 + 36\omega_0^2)} e^{bt/2} \cos \omega_0 t + \frac{12\omega_0^2 b}{a(b^2 + 36\omega_0^2)} e^{bt/2} \sin \omega_0 t \\ &\quad + \frac{24\omega_0^3}{a(b^2 + 36\omega_0^2)}. \end{aligned}$$

We now have the following representations for $R_{11}(t)$ and $R_{21}(t)$.

$$\begin{aligned} R_{11}(t) = & -\frac{e^{bt/2}}{3\omega_0^3} \sin^3 \omega_0 t - \frac{b}{3\omega_0^3} \left(\frac{1}{b^2 + 36\omega_0^2} \right) \{ e^{bt/2} (2b \sin^3 \omega_0 t \\ & - 12\omega_0 \sin^2 \omega_0 t \cos \omega_0 t - \frac{24\omega_0^3 \cos \omega_0 t}{a} + \frac{12\omega_0^2 b \sin \omega_0 t}{a}) + \frac{24\omega_0^3}{a} \} \end{aligned}$$

$$\begin{aligned} R_{21}(t) = & \frac{1}{a\omega_0} [e^{bt/2} (\frac{b}{2} \sin \omega_0 t - \omega_0 \cos \omega_0 t) + \omega_0] \\ & - \frac{a}{\omega_0^3} \left(\frac{1}{b^2 + 36\omega_0^2} \right) \{ e^{bt/2} (2b \sin^3 \omega_0 t \\ & - 12\omega_0 \sin^2 \omega_0 t \cos \omega_0 t - \frac{24\omega_0^3 \cos \omega_0 t}{a} \\ & + \frac{12\omega_0^2 b \sin \omega_0 t}{a}) + \frac{24\omega_0^3}{a} \}. \end{aligned}$$

It follows from the above representations for $R_{11}(t)$, $R_{21}(t)$, and (F.10) that

$$x_2(t) = -e^{At}(p^0)^2 c \begin{bmatrix} R_{11}(t) \\ R_{21}(t) \end{bmatrix}$$

$$\begin{aligned}
&= -c(p^0)^2 e^{At} \left\{ \left[\frac{-(3b^2 + 36\omega_0^2)}{-6ab} \right] \frac{\sin^3 \omega_0 t}{3\omega_0^3(b^2 + 36\omega_0^2)} e^{bt/2} \right. \\
&+ \left[\frac{4b}{12a} \right] \frac{\sin^2 \omega_0 t \cos \omega_0 t}{\omega_0^2(b^2 + 36\omega_0^2)} e^{bt/2} \\
&+ \left[\frac{-b^2 - 36\omega_0^2 + 24a}{(b^2 + 36\omega_0^2)a} \right] \frac{\cos \omega_0 t}{(b^2 + 36\omega_0^2)a} e^{bt/2} \\
&+ \left[\frac{-8b^2}{b^3 + 36b\omega_0^2 - 24ab} \right] \frac{\sin \omega_0 t}{2a\omega_0(b^2 + 36\omega_0^2)} e^{bt/2} \\
&\left. + \left[\frac{-8b}{b^2 + 36\omega_0^2 - 24a} \right] \frac{1}{a(b^2 + 36\omega_0^2)} \right\}.
\end{aligned}$$

Appendix G

SMP Function for Volterra Equations Calculations

The SMP function used to generate the differential equations for the Volterra series terms is listed in Figure A1. The nonlinear differential equation is assumed to be of the form

$$\dot{x} = f(x, u)$$

The inputs to the function are:

$$f = \{f_1, f_2, \dots, f_n\} = \text{components of } f(x, u).$$

$$var = \{x_1, \dots, x_n, u\} = \text{list of state variables and the input variable (last).}$$

$$eq = \text{list of equilibrium values of the variables in } var.$$

$$ord = \text{number of Volterra series terms to be generated.}$$

A sample output of the program for the wing rock example is shown in Figure A2.

This function implements the procedure outlined in Section II. A line-by-line description of the function follows.

1. n is set equal to the order of the system.
2. sub is set equal to the substitution list.

$$var_i \rightarrow \sum_{j=1}^{ord} var_i[j](a)^j + eq_i \quad i = 1, \dots, n$$

$$var_{n+1} \rightarrow (a)var_{n+1} + eq_{n+1}$$

3. fs is a set equal to f with the above substitutions.
4. Technical detail. $Ar[\cdot]$, a projection that converts truncated series expansions into polynomials, is forced to distribute over lists.

5. The function $\%fs$ is expanded in a Taylor series with respect to the dummy variable $(\%a)$ up to order $\%ord$.
6. For each Volterra series term $x[i], \frac{dx[i]}{dt}$ is set equal to the coefficient of $(\%a)^i$ in the expansion of $\%fs$.

```

/*:volt[$f,$var,$eq,$ord]
   gives differential equations for the components of the state
   corresponding to terms in the volterra series for the state
   equation dx/dt=$f(x,u). The state variables and input variable
   are listed in $var with the input variable listed last. $eq
   is a list of the equilibrium values of $var, and $ord is the
   number of terms in the volterra series to be considered. */

volt[$f,$var,$eq,$ord]:\
  (%n:Len[$f]);\
  %sub:Cat[Ar[%n,$var[$1]]->Sum[[$var[$1]][i] %a-i,(i,1,$ord)]\
    +$eq[$1]],[$var[%n+1]]->%a $var[%n+1]+$eq[%n+1]]);\
  %fs:S[$f,%sub];_Ax[Ldist]:1;%fe:Ax[Ps[%fs,%a,0,$ord]];\
  Do[i,1,$ord,Do[j,1,%n,Pr["d/dt",[$var[j]][i],"=",\
    N[Col[Ex[Coef[%a-i,%fe[j]]]]]]];Pr[];Pr[]))

```

FIGURE A1. SMP Function

SMP 1.5.0
23-JUL-1987 08:57:41.05

```

#I[1]:: f:(p,-26.6667 phi+.76485 (1-3.82 phi ) p)

#O[1]:: (p,-26.6667phi + 0.76485p (1 - 3.82phi))

#I[2]:: <volterra

#I[3]:: volt[f,(phi,p,u),(0,0,0),5]

d/dt   phi[1] =      p[1]
d/dt   p[1]   =      0.76485p[1] - 26.6667phi[1]

d/dt   phi[2] =      p[2]
d/dt   p[2]   =      0.76485p[2] - 26.6667phi[2] - 2.92173p[1] phi[1]

d/dt   phi[3] =      p[3]
d/dt   p[3]   =      0.76485p[3] - 26.6667phi[3] - 2.92173p[1] phi[2]
                        - 2.92173p[2] phi[1]

d/dt   phi[4] =      p[4]
d/dt   p[4]   =      0.76485p[4] - 26.6667phi[4] - 2.92173p[1] phi[3]
                        - 2.92173p[2] phi[2] - 2.92173p[3] phi[1]

d/dt   phi[5] =      p[5]
d/dt   p[5]   =      0.76485p[5] - 26.6667phi[5] - 2.92173p[1] phi[4]
                        - 2.92173p[2] phi[3] - 2.92173p[3] phi[2]
                        - 2.92173p[4] phi[1]

#I[4]:: Exit[]

```

FIGURE A2. OUTPUT FOR THE WING ROCK EXAMPLE